Burning Behavior of Oil in Ice Cavities

Final Report

Prepared by:

Ali S. Rangwala (PI)
Associate Professor,
Department of Fire Protection Engineering,
Worcester Polytechnic Institute
Worcester, MA 01609

Albert Simeoni (Co-PI)
BRE Center for Fire Safety Engineering,
University of Edinburgh
Edinburgh, EH9 3JL, UK

Dr. Shi Xiaochuan
Research Scientist
Department of Fire Protection Engineering
Worcester Polytechnic Institute

BSEE Contract No. E12PC00056

Date: 30 December 2013

Acknowledgements

This study is funded by the Bureau of Safety and Environmental Enforcement, US Department of the Interior, Washington, D.C., under Contract Number E12PC00056. The authors would like to thank George S. Trifon, Timothy Steffek, Hung Nguyen and Herma Banks for support and coordination during this study.

Many thanks to WPI personnel, who made contributions during this study, including:

Peter Bellino (graduate student), Hamed Farmahini (graduate student), Brian Elias (graduate student), Minkyu Lee (graduate student), Sreenivasan Ranganathan (graduate student), Ying Zou (graduate student), Minchao Yin (graduate student), Haoran Li (undergraduate student), Andre Da Vitoria (undergraduate student), Sowmit Barua (undergraduate student), Randy Harris (WPI fire laboratory manager), and Kevin Arruda (lab machinist).

Summary

In-situ burning (ISB) is a practical means of oil spill cleanup in icy conditions. The controlling parameters related to *in-situ* burning in icy conditions are currently unknown. The scientific problem involves new fundamental studies about the interaction of a pool of oil burning in a matrix made of ice. This interaction represents the innovative aspect of this work that has not been studied before and in a broader sense forms the main deliverable of the project.

This study considers one example of an oil spill scenario: burning oil in an ice cavity. A new set of parameters to the classical problem of confined pool fires in vessels arises under these unique conditions. The icy walls of the cavity create a significant heat sink causing considerable lateral heat losses, especially for the small cavity sizes. Melting ice because of the heat from the flame causes the cavity geometry to change. Specifically, the diameter of the pool fire increases as the burning advances. This widening causes the fuel to stretch laterally reducing its thickness at a faster rate. The melted ice water causes the oil layer to rise, which causes the ullage height to decrease. The drop in ullage and increase in diameter counteract the decrease in thickness because of the widening. This results in a strong coupling between the mass loss rate ($\dot{m}$) and the geometry change of the pool and cavity.

To systematically explore this process, experiments were performed in circular ice cavities of varying diameters (5 cm to 100 cm). The experiments were divided into 3 types based on size or diameter of the initial ice-cavity: small scale tests (~ 5 – 15 cm), intermediate scale tests (15 – 30 cm) and large scale (~1m). It was found that because of the cavity expansion the average $\dot{m}$ of crude oil in the ice cavity is greater than the $\dot{m}$ in a similar sized vessel. A systematic analysis of the experimental data allows the separation of the burning rate into parts caused by convection, radiation, conduction (laterally and in-depth) and other heat transfer mechanisms towards development of an engineering predictive model. The model predicts mass loss rates and shows reasonable agreement with the experimental results. Limits of the model are discussed.

1. Outline

The efficiency of *in situ* burning for oil spills on water is predominantly controlled by the thickness of the oil spill and wind conditions. However, the controlling parameters related to in-situ burning in icy conditions are unknown. Burning behavior of combustible liquids (octane and crude oil) in an ice cavity in small-scale (5 cm diameter), intermediate scale (~30 cm diameter), and large-scale (~ 100 cm diameter) have been investigated. A model is developed to predict the burning rate based on the small-scale test results, and then reassessed by large-scale test results.

This report is organized as:

- *Section 2* presents the scientific approach using small, intermediate and large scale experiments to explore the problem of oil burning in an ice cavity.
- *Section 3* presents experimental results for the small scale testing using 5 cm diameter vessels and ice-cavities (5 and 10 cm). Experimental results with Alaska North Slope (ANS) crude oil are analyzed.
- *Section 4* presents the results obtained using the intermediate scale tests. In this case, both ice cavities (~15-25 cm diameter) and ice channels (65 cm long, 16 wide and 10 deep) are analyzed.
- *Section 5* presents the experimental results obtained from the large scale oil burn in a 1.1 x 1.1 m^2 square and 0.16 m deep ice cavity.
- *Section 6* compares the burning dynamics of small, intermediate and large-scale experiments
- *Section 7* presents the formulation of the mathematical model.
- *Section 8* presents the conclusions and future work.

The properties of combustible liquids used in this study are provided in Appendix A. Baseline test data for the fuels tested is provided in Appendix B. The spread of an oil slick on water and ice channels is presented in Appendix C. The large-scale test protocol performed on 9/25/2013 is presented in Appendix D. References cited in this report are listed at the end.

2. Approach

The fundamental problem of burning oil in an ice-cavity is new to the fire science community and there are no prior experiments to formulate a plan of study. The approach used to explore the problem was therefore based on physically understanding the problem using several experiments performed at the small-scale and intermediate scale which are low-cost, easy to control and instrument. The small-scale experiments mainly comprised of 5 and 10 cm diameter ice cavities and vessels of different fuels such as Octane, Xylene and Alaska North Slope (ANS) crude oil. Octane, a single component low flash point fuel represents the high volatile-fraction of a typical crude oil. Xylene, a single component, high flash point fuel with significant sooting tendency represents the low-volatile, aromatic content in a typical crude-oil fire. Finally, ANS crude represents a realistic muticomponent fuel mixture. After completion of several small-scale tests, the model fire behavior was extrapolated to the full-scale as shown in Fig. 1 using a progression of sizes in the test configurations.

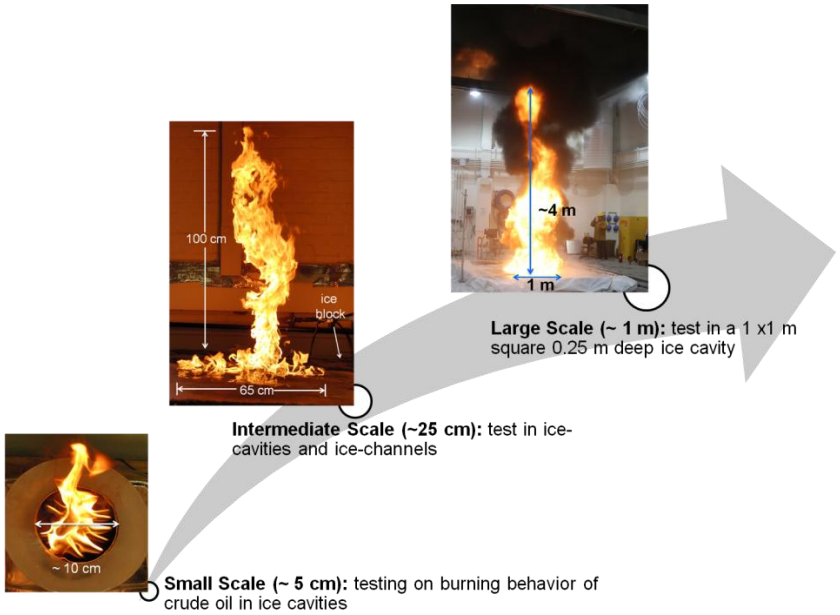

Fig. 1: Experiments at small, intermediate and large-scale.

Figure 1 shows the progression of experimental testing that was adopted in this study. Initial test were performed in ice-cavities with a diameter of 5 to 10 cm. Such small-scale tests were performed to identify the controlling parameters governing the mass burning rate of a fuel in an ice-cavity. These tests were followed with larger ice-cavity sizes of 15 – 25 cm range and ice channels 65 cm long, 16 cm wide and 10 cm deep and ultimately with a large-scale test comprising of a 1 m^2 square ice cavity, 25 cm deep as shown in Fig. 1. The approach allowed development of scaling relationships by the separation of the mass burning rate into parts caused by conduction, convection, radiation and other heat transfer mechanisms. The advantage of the approach is that since a full-scale test is prohibitive in cost, a large number of tests can be performed at the bench scale and intermediate scale and the primary controlling parameters such as fuel type, thickness, geometry can be varied to obtain a fundamental understanding of the problem. Instrumentation is also easier at the small-scale and several repeat tests can be performed to test the accuracy of the measurements. The information is then used towards understanding the results of the full-scale test in a meaningful way.

3. Experimental results and discussion for tests at the small (bench) scale (~5 -10 cm)

3.1 Burning of a liquid fuel in a container surrounded by salty ice water

Preliminary experimental results with the pool size ranging from 3 to 8 cm showed that a 4.5 – 5 cm initial diameter is necessary to obtain sustained combustion of ANS crude oil used in this study. This is because heat losses to the surrounding vessel wall maintained between 20 ºC to -10 ºC are too high to sustain continuous burning for diameters less than 4.5 cm. Figure 2 shows a diagram and a photograph of the experimental setup. An aluminum tube (0.1 cm wall thickness) with inner diameter of 4.8 cm is determined as a pool size.

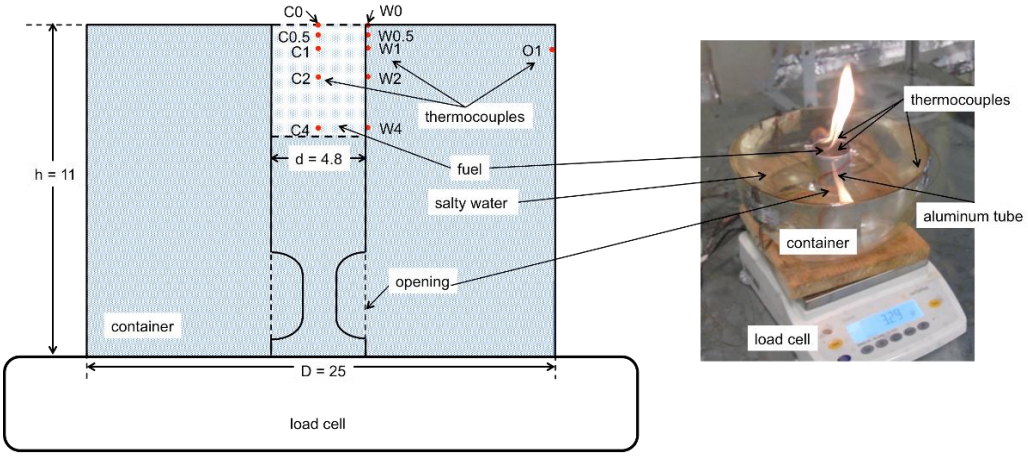

Fig. 2: Experimental setup for burning behavior of a fuel in a vessel surrounded by icy water. All the dimensions are in cm; thermocouples are labeled by their locations (center or wall and distance). For example, "C4" represents a thermocouple along the centerline located 4 cm below the fuel surface.

As shown in Fig. 2, thermocouples (type K, gauge 36) along the centerline of the tube are labeled "C", while thermocouples on the outside wall of the tube are labeled "W". The numbers following "C" or "W" denote the distance from the top of tube rim to a certain thermocouple. Temperature of the surrounding water/salty ice water (faraway from the burning tube) is measured by a thermocouple "O1" placed on the inside wall (1 cm below the rim) of the outer container. All thermocouples record temperatures at a sampling rate of 1 data point per second using a National Instrument "NI cDAQ-9174" which comprises of 16 thermocouple channels per module (4 modules). All thermocouples are welded using an Omega Thermocouple and Fine Wire Welder "TL-WELD".

Tests are conducted with the surrounding water (filled in the container) at room temperature 20°C and with the salty ice water around -10°C, respectively. The low surrounding temperature is achieved using 20 grams of rock salt added into every 100 grams of water. After 24 hours in a freezer, the salty water could reach down to -18°C while remaining in liquid phase. Then the solution is placed in room temperature environment. After an hour the solution reaches to -10 °C and remains at this temperature for 3 hours thus providing controllable initial condition. Octane or crude oil with various thicknesses (0.4, 1 and 2 cm (and 4 cm for crude only)) are added to the vessel and ignited using a butane torch. For the low temperature cases, the fuels were kept in a separate -10 ºC bath to ensure equal temperatures of fuel and surroundings before ignition. Ignition is quick and the entire surface ignited within 1 s for all cases. The initial fuel surface always touched the thermocouple C0 and thus for all cases, the

surface of the fuel is between C0 and C1. Temperature profiles were recorded by thermocouple arrays located as shown in Fig. 2 by the red dots. A load cell (Sartorius "ED 6202S-CW" l precision of 0.01 g and 5 data points per second) is used to record the mass loss rate. Other parameters that are measured include flame height, time to extinction, and thickness of fuel layer at extinction. Experiments were repeated 3 times and good repeatability was observed between tests. This is further discussed in section 3.2. The experimental for octane and ANS crude oil are shown in Table 1.

Table 1: Experimental results for octane and ANS crude in a 4.8 cm diameter vessel surrounded by water at 20ºC and -10ºC

Test #	Fuel type	Surrounding temperature	Fuel thickness [cm]	Total fuel [g]	Mass loss [g]	Burn efficiency [%]	Burn duration [s]	Fuel thickness at extinct [cm]
1	octane	room (20ºC)	0.4	4.33	6.22	100*	406	N/A
2	octane	room	1	12.11	18.28	100*	1288	N/A
3	octane	room	2	24.97	40.10	100*	1294	N/A
4	crude oil	room	0.4	4.67	1.56	33.40	157	0.27
5	crude oil	room	1	14.16	5.66	39.97	498	0.60
6	crude oil	room	2	29.40	13.20	44.90	1079	1.10
7	crude oil	room	4	54.78	27.40	50.02	2197	2.00
8	octane	low (-10ºC)	0.4	4.60	–	–	52	–
9	octane	low	1	12.33	–	–	423	–
10	octane	low	2	24.85	10.01	40.28	1921	1.19
11	crude oil	low	0.4	4.85	0.95	19.59	174	0.32
12	crude oil	low	1	–	–	–	–	–
13	crude oil	low	2	29.92	7.23	24.16	1111	1.52
14	crude oil	low	4	–	–	–	–	–

*Burning efficiency of octane in room temperature water is 100%. The total mass loss is more than the total fuel mass because of the water evaporation loss.

Table 1 shows that the burning efficiency (mass loss x 100 / initial mass) of both octane and ANS crude oil is significantly lowered (~40%) under low temperature conditions. This is further shown in Fig. 3 where the mass loss rate of ANS crude oil is plotted as a function of time. Fig. 3 shows the mass burning rate is a function of the initial thickness of the fuel layer similar to the results of Garo et al. [1]. For 2 cm thick layer the mass loss rate is higher compared with the 4 mm thickness. For the current experimental conditions, 4 mm was the critical thickness. The crude oil could not be ignited below this limit for the -10ºC temperature condition. The trend of the mass loss rate for similar thicknesses is similar, however, quantitatively lower as the temperature is decreased.

This is important to note and the result can be used to develop scaling relationships with temperature. Fig. 3 shows that the mass loss rate gradually decreases for the 2 cm thick fuel layer while for the 4 mm thickness it increases initially for the first 50 s and then drops sharply. This is most likely because of the multicomponent nature of the ANS crude oil. The intersection of the horizontal dashed lines with the Y-axis denotes the critical mass loss rate or the mass loss rate at extinction. It is interesting to note the critical mass loss rate of ANS crude oil is similar for both 4 mm and 2 cm initial thicknesses when the surrounding temperature is -10 ºC.

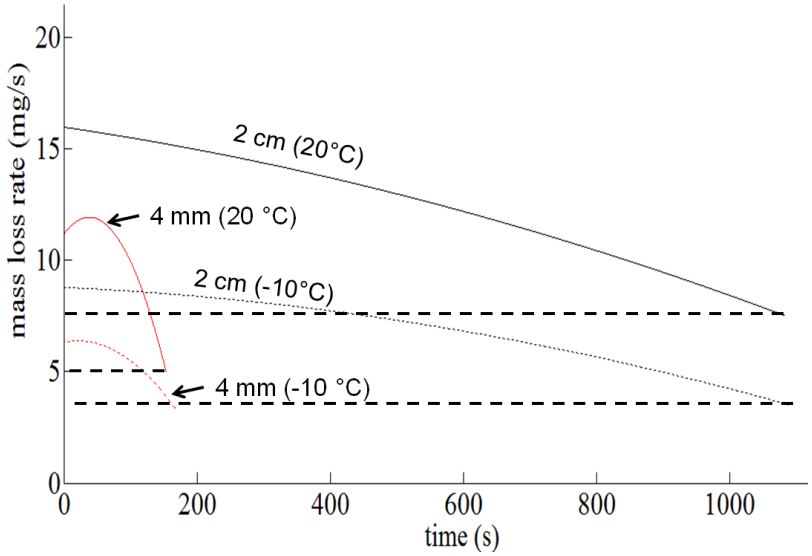

Fig. 3: Burning behavior of ANS crude oil at initial thickness of 4 mm and 2 cm at ambient (20ºC) and cold temperatures (-10ºC). The horizontal dashed lines show critical mass loss rate at extinction.

Figure 4 shows a comparison of the burning behavior between ANS crude oil with octane. Once again, as surrounding temperature is lowered, the mass burning rate is lowered and the percentage decrease in octane and crude is similar. The mass loss rate of octane is almost constant throughout the experiment and slightly increases at later times. This is mainly because of the aluminium rim heating up after such long times. However, for crude the mass loss rate decreases and this is mostly because of its multicomponent nature. As the burning continues, the lighter volatiles evaporate away leaving the heavy volatiles behind. The flame size is not significant enough to sustain vaporization of the heavy volatiles at the same rate which is why the mass loss rate decreases.

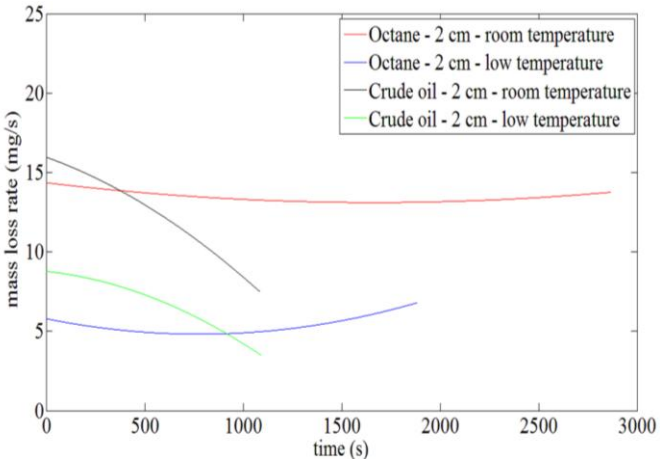

Fig. 4: Comparison of burning behavior of octane and crude oil. Initial thickness = 2cm.

Figure 5 shows the temperature profiles for octane recorded by the thermocouples shown in Fig. 2. The solid lines denote the temperature along the centerline of the tube, and the dotted line denotes the temperature on the outside wall of the tube. Lines in red, blue, yellow, green, and purple denote the location of the thermocouples as 0 cm, 0.5 cm, 1 cm, 2 cm, and 4 cm below the fuel surface level, respectively.

For the burning of octane with 0.4 cm layer thickness in room temperature water (Figure 5 a, left), the temperature of C0 is in the range of 80 - 90°C, which is below the boiling point (125°C) of octane. 0.4 cm octane layer surface stayed at the level of C0 during the burning and was self-extinguished after about 400 s. For the burning of octane with 1 cm layer thickness (room temperate), the temperature of C0 shows a sharp increase from 90°C to around 400°C (not shown on plot) at 426 s after ignition. Fuel surface after this time was below C0. After about 1300 s, fuel surface reached the location of thermocouple C0.5 right before the self-extinguishment. Since we are more interested in the fuel temperature distribution, all the plots for octane are scaled from 0 – 125°C (boiling point of octane). For the burning of octane with 2 cm layer thickness, the fuel surface went below C0 at 426 s, similar to 1 cm burn, and reached the C0.5 at 990 s.

The initial temperature for the octane burning in icy water was approximately -10°C. Octane was self-extinguished in a shorter time period for both 0.4 and 1 cm thicknesses compare to the burn in room temperature water. This is due to the larger heat loss from small amount of fuel to the low temperature surrounding (icy water) than to the room temperate surrounding. Octane burn with 2 cm layer thickness with icy water showed longer burning duration than the burning in room temperature water, but a much lower mass loss rate (3 ~ 6 mg/s versus 12 ~ 15 mg/s as burning in room temperature water as shown in Fig. 4).

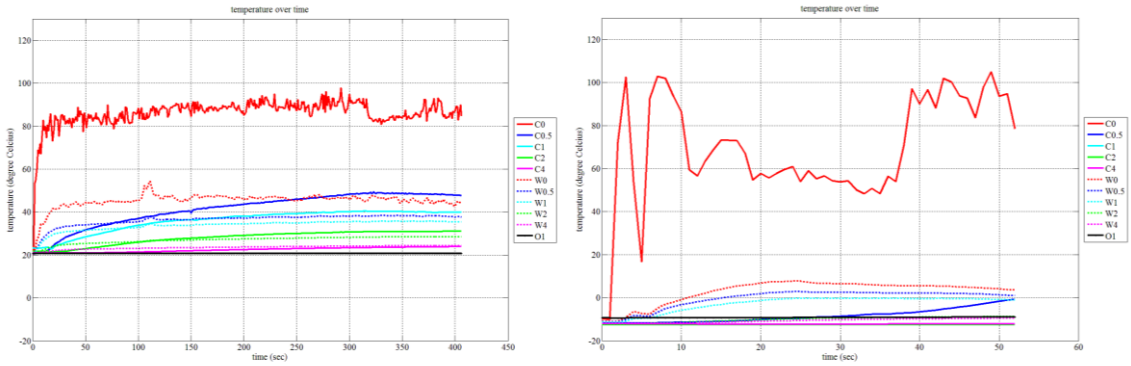

a) Octane layer of 0.4 cm thickness: room temperature water (left) & -10°C salty water (right)

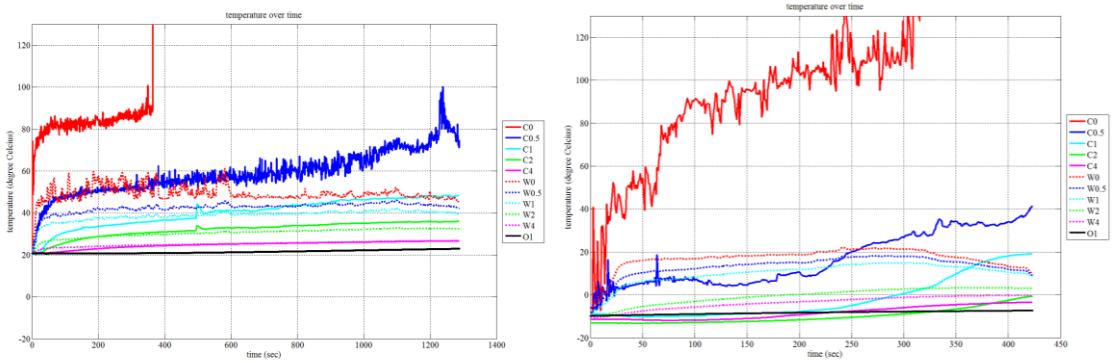

b) Octane layer of 1 cm thickness: room temperature water (left) & -10°C salty water (right)

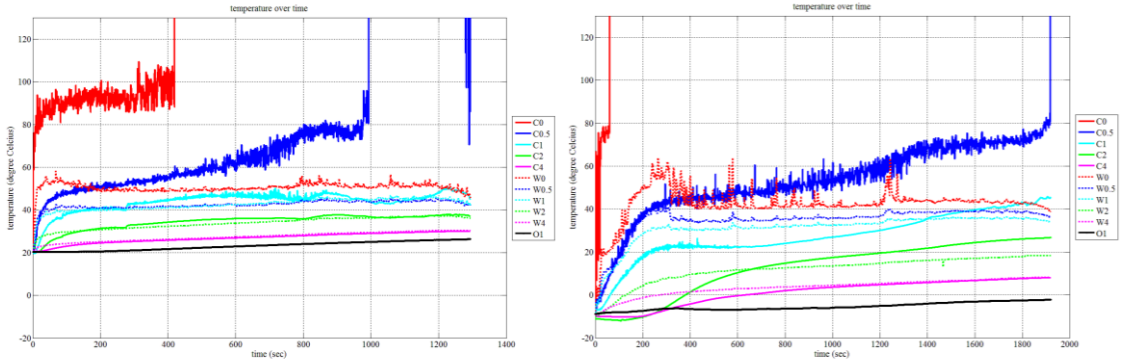

c) Octane layer of 2 cm thickness: room temperature water (left) & -10°C salty water (right)

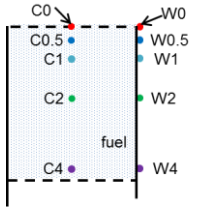

Fig. 5: Temperature vs. time of octane burned with various oil thicknesses, surrounded by room temperature (20 ºC) water and -10 °C salty water.

Figure 6 shows the spatial temperature profiles for octane at different time intervals starting from ignition to extinction. Each plot consists of two subplots: upper one shows the temperature profile at the center of the tube and the bottom one shows the temperature profile of the tube wall. In all plots, the first line (red) shows the temperature profile at t = 0 seconds, which is the temperature before ignition.

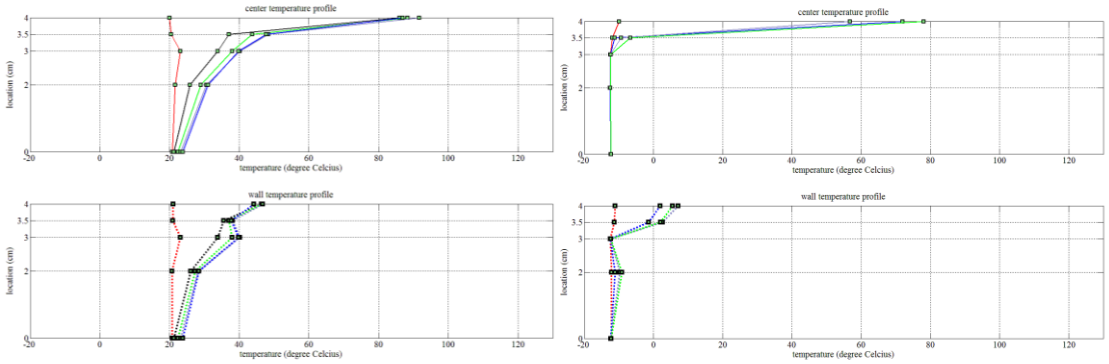

a) Octane layer of 0.4 cm thickness: room temperature water & -10°C salty water

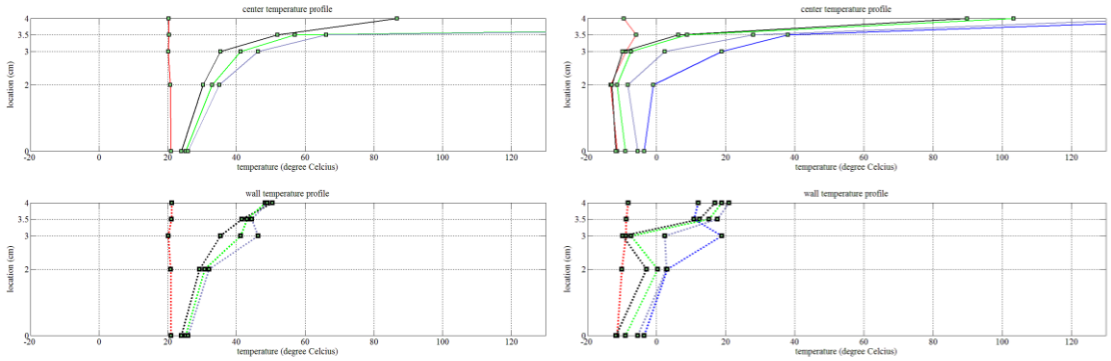

b) Octane layer of 1 cm thickness: room temperature water & -10°C salty water

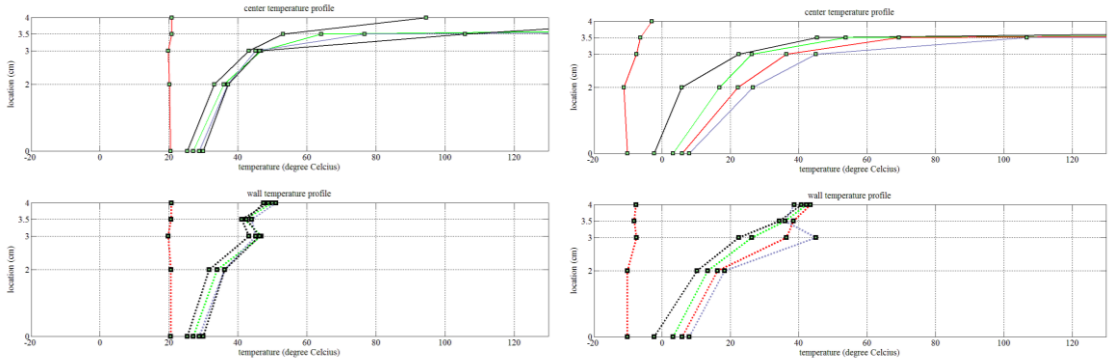

c) Octane layer of 2 cm thickness: room temperature water & -10°C salty water

Fig. 6: Octane temperature vs. location with various oil thicknesses, surrounded by room temperature water and -10°C salty water.

3.2 Repeatability analysis

To study the repeatability of the experiments, three tests on burning of octane with 4 mm layer thickness in room temperature water are conducted, and the results are shown in Fig. 7 – 10.

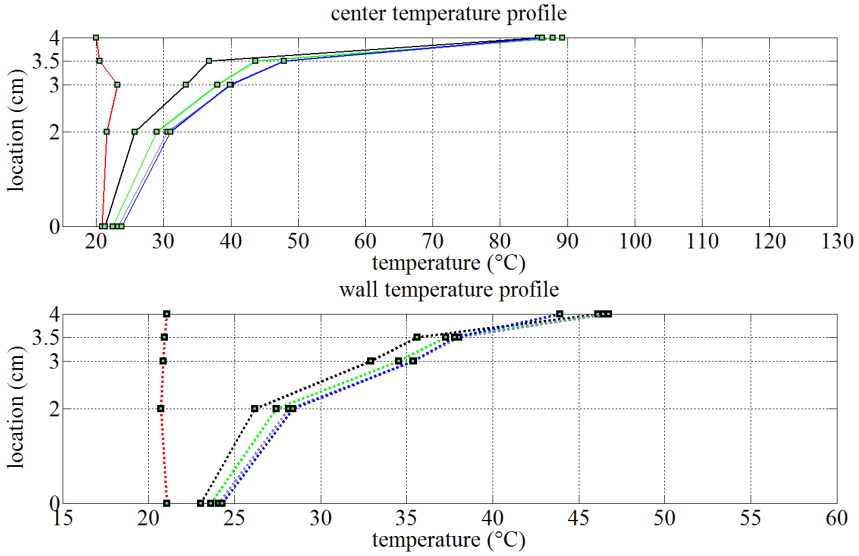

Fig. 7: Octane – 4 mm – room temperature water – trial 1

Time step from left to right: 0, 101, 202, 303, 404 s (test #1)

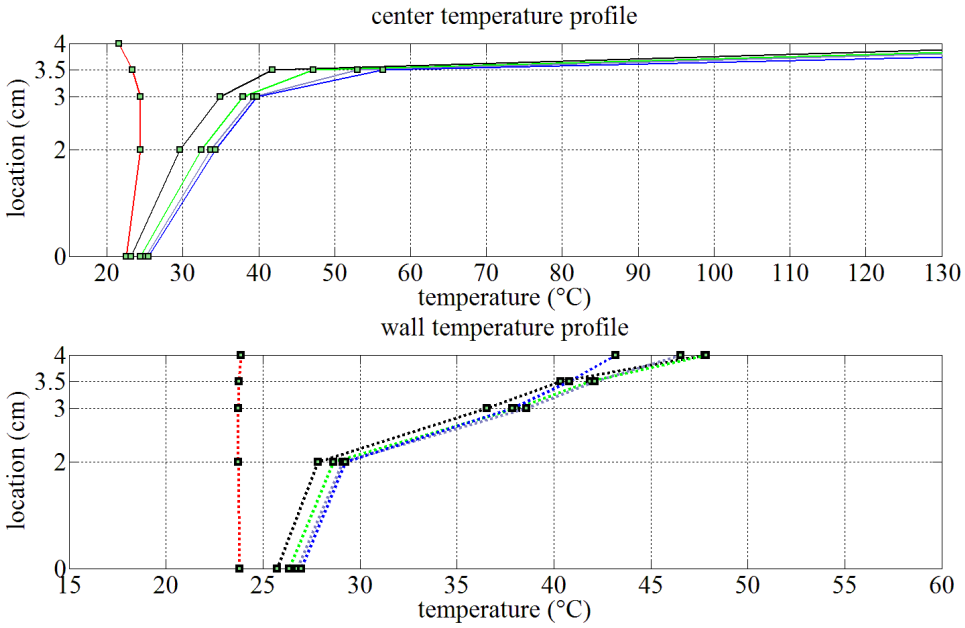

Fig. 8: Octane – 4 mm – room temperature water – trial 2

Time step from left to right: 0, 129, 258, 387, 516 s (test #15)

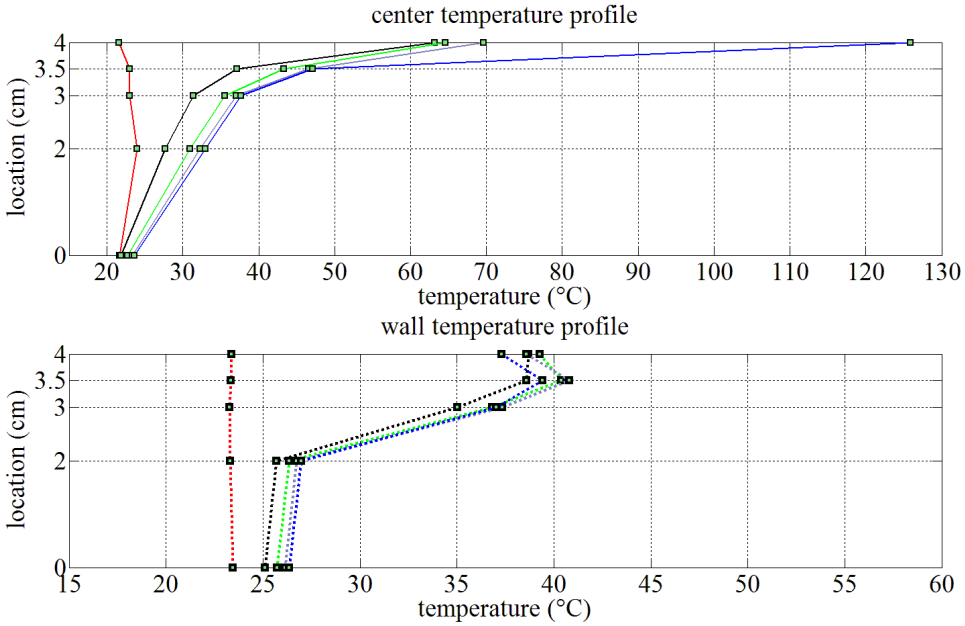

Fig. 9: Octane – 4 mm – room temperature water – trial 3

Time step from left to right: 0, 103, 206, 309, 412 s (test #16)

As shown in Fig. 7 - 9, the temperature profiles are similar to one another for three different tests with the same parameter: thickness of fuel = 4 mm. The only difference is on temperature at W0. For test 16, the temperature recorded by W0 is lower than that of test 1 and test 15. This may be because of the shifting of the thermocouples during the experiments. The contact resistance of the thermocouple with the wall is maintained using omega thermocouple cement. This may have chipped off during one of the trials. The comparison of mass loss rate (not shown) also shows good repeatability. The standard deviation for burning efficiency is less than 10%.

3.3 Burning of a liquid fuel in an ice cavity

The experimental setup used to study the burning behavior of a fuel in an ice cavity was studied next. Compared with the confined pool fire case analyzed in section 3.1, the shape of the ice-cavity evolves as the burning progresses because of melting ice from the flame heat flux. To explore the problem, experiments were conducted in circular ice cavities with varying diameters (5 – 25 cm). The experiments with cavity sizes of 5 – 10 cm are reported in this section and those at 15 and 25 cm are reported in Section 4. The change in the shape of the ice cavity and the oil layer thickness are recorded using a combination of visual images, mass loss, and temperature data along the centerline and the wall of the cavity. The experimental setup is shown in Fig. 10.

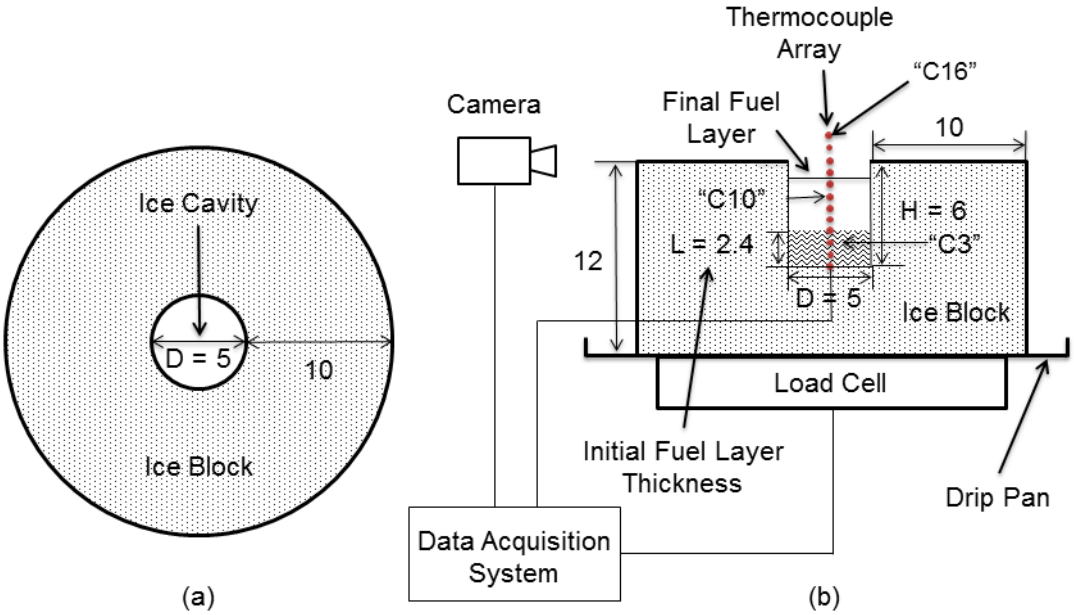

Fig. 10: Experimental setup. (a) Top view and (b) side view. All dimensions in cm.

The ice blocks with *D* = 5 and 10 cm were equipped with Thermocouples (type K, gauge 36, diameter of 0.13 mm) to acquire a temperature profile of the liquid layer to use in the predictive model. Sixteen thermocouples, installed on one array, were utilized to record the temperature at different elevation (0.5 cm apart) and obtain temperature of fuel surface and fuel-water interface along centerline of cavity. Thermocouples are shown in Fig. 10, along the centerline of the cavity with small solid circles. ANS crude oil was allowed to burn to extinction in a quiescent environment. Crude oil is a complex mixture of hydrocarbon of various molecular weights and shows a transient set of properties i.e. boiling point of ANS crude oil varies from 38 °C to 570 °C. Table 2 lists the relevant properties of crude oil.

The experimental procedure comprised of placing the ice block on the load cell then pouring liquid fuel at a certain height (at initial temperature of 20°C) and igniting it immediately. The igniter was held 3 seconds for all trials. All trials were allowed to burn to extinction.

Table 2: ANS crude oil properties at 25°C

Liquid Density (kg/m^3)	866
Viscosity (centi-poise, cP)	11.04
Flashpoint (°C)	25 – 35
Boiling Point (°C)	38 – 570
Thermal Conductivity λ (W/m K)	0.09 - 0.14
Specific Heat, C_p(kJ/kg K)	2.2
Latent Heat L_v (kJ/kg)	250

Figure 11 shows the main dimensions that can influence the burning-rate of a fuel in an ice cavity. Four dimensions: diameter (*D*), height (*H*), fuel thickness (*L*) and the depth of the fuel surface defined as ullage (*U*) can influence the burning behavior. If there exists an initial layer of water below the fuel, then the initial thickness of the water sublayer may also influence the problem. However, this was not studied for the small-scale tests and in all small and intermediate scale experiments there exists no initial water sublayer.

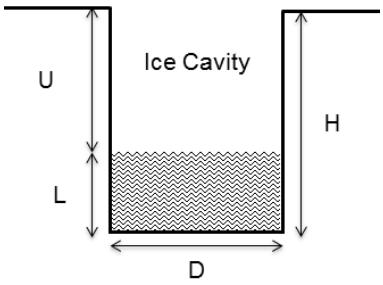

Fig. 11: Dimensions of cavity.

When a liquid fuel is burned in a confinement such as a vessel of diameter (*D*) the ullage (U) increases as the liquid is consumed. However, burning in ice cavities is different because the ice melts because of flame heat flux and similarly causes water accumulation in the ice cavity. Because of melting of ice and accumulation of water underneath the fuel layer, the fuel layer rises, causing the ullage to decrease. This behavior results in two possible extinction scenarios for burning of the liquid fuels in an ice cavity:

1. Natural extinction where the fuel layer does not reach the ice surface and extinguishes because of attainment of a critical layer thickness, where sufficient vaporization is not possible because of heat losses. This behavior is similar to that reported by Wu et al. [2] and is the commonly observed extinction phenomena in oil slick fires in water. This extinction is shown in Fig. 12 a.
2. The second extinction is because of the rapid change in geometry of the cavity because of melting of ice and corresponding water formation. The accumulation of water underneath the fuel layer can result in spillage of the fuel out of the cavity because of rapid melting of water. This makes the confined spill bounded by the cavity walls into an unconfined spill scenario. The fuel pouring out of the cavity forms a thin fuel layer on the ice surface which extinguishes quickly. This behavior is relatively unexplored in fire science literature. This type of extinction is shown in Fig. 12 b.

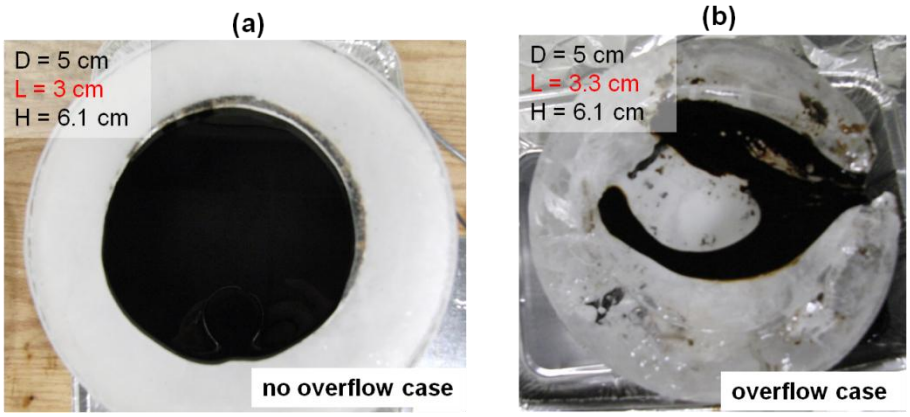

Fig. 12: Extinction scenarios: (a) Case where oil is confined in the cavity and extinguished because of attainment of a critical thickness (~3mm), and (b) extinction observed due to overflow. ANS crude oil, D = 5 cm.

In this exploratory study, it was decided to explore conditions necessary for natural extinction alone. A **critical ratio** defined as height of cavity/fuel layer thickness was established using octane and ANS crude to denote the threshold where spillage of fuel out of the cavity is experimentally observed. A series of preliminary tests with different cavity heights and fuel layer thicknesses were performed to establish the critical ratio. Further tests were then performed such that the burning never resulted in fuel spillage out of the cavity. In other words, the depth (*H*) and fuel layer thickness (*L*) were chosen based on the data obtained from preliminary tests to prevent overflow and spillage during combustion. Table 3 summarizes the dimensions for such preliminary tests. As shown in Table 3 for *D* = 5 cm the ratio (*L/H*) should be less than 0.5 in order to avoid fuel spillage out of the cavity because of melting of ice. The *L/H* ratio for octane (*D* = 5 cm) equals 0.4, showing the spill-out of the cavity is a function of the nature or type of fuel. Once this threshold was established, in all further tests the cavity height was always maintained at a value such that *L/H* < 0.5 for ANS crude and *L/H* < 0.4 for octane. The initial fuel layer thickness for all trials were selected to be ~1.5 cm based on prior studies [2-4] stating the minimum required thickness of oil slick needs to be between 1cm and 2 cm to have successful burning.

Table 3: Critical *L/H* ratio to avoid fuel spillage (ANS crude oil)

ANS crude oil	Initial ullage (U) (cm)	Initial fuel layer thickness (L) (cm)	Depth (H) (cm)	Critical ratio L / H (cm)	Final ullage (cm)
D = 5 cm	4	2.1	6.1	0.34	1.2
D = 5 cm	3.6	2.4	6	0.4	0.7
D = 5 cm	3.1	3	6.1	0.5	0.3
D = 5 cm	2.8	3.3	6.1	0.54	Over flow

Once critical ratios were determined, a total of 12 tests (6 with octane and 6 with ANS crude) were performed (3 tests each for 5 cm and 10 cm diameters). Table 4 shows the experimental results for crude oil and octane burn in an ice cavity with *D* = 5 cm. Three repeated trial are conducted for each fuel.

Table 4: Experimental results for burning of crude and octane in an ice cavity (5 cm)

	Average MLR (g/s)	Maximum MLR (g/s)	Burn Efficiency (%)	Fuel Layer Thickness at Extinction (cm)	Diameter of Cavity at Extinction (cm)	Length of Lip (cm)
Crude 1	0.0174	0.0274	24.31	0.29	11.5	0.75
Crude 2	0.0161	0.0364	31.07	0.25	13.5	1
Crude 3	0.0141	0.044	33.01	0.21	15	0.75
Octane 1	0.034	0.052	97.70	0	19	- (melted top)
Octane 2	0.026	0.041	59.30	0.07	16	2
Octane 3	0.029	0.049	60.06	0.06	17	2

Table 4 shows that the average mass loss rate for crude oil is 66% lower than octane. An average burn efficiency of 60% is observed for octane while the average efficiency for ANS crude oil is ~30%. In the presence of ice, the temperature of fuel layer is significantly lower because of heat loss to the walls and water below. This could be the main reason for the reduced burning efficiency. Experiments also show that a significant amount of oil is trapped underneath a lateral cavity formed during the burning. One trial of octane has 98% burn efficiency, compared with 60% (Trial #1, octane, Table 4). In this case, although the lateral cavity was formed, it melted away during the burn. The physical reason for the onset of cavity formation is not clearly understood and further work is necessary to clearly investigate this phenomena.

Mass loss rate

Figure 13 shows the mass loss data for octane and ANS crude oil trials respectively. It is observed that, crude oil has a shorter burning time and smaller intensity in a similar conditions compared with octane. It is interesting to note the difference in the trends of mass loss rate between the confined vessel surrounded by water (Section 3.1) and the ice cavity. As shown in Fig. 3, when ANS crude oil is surrounded by icy-cold water, but contained, its burning rate decreases with time. However, when surrounded by an ice-cavity, its burning rate increases and then decreases sharply close to extinction. The peak burning rate in ice cavity (0.05 g/s as shown in Fig. 13) is nearly 5 times higher (~0.01 g/s as shown in Fig. 3). This difference is mainly because of the melting of ice which causes the overall diameter of the spill to increase. However, as the diameter of the spill increases, it also becomes thinner by causing early extinction.

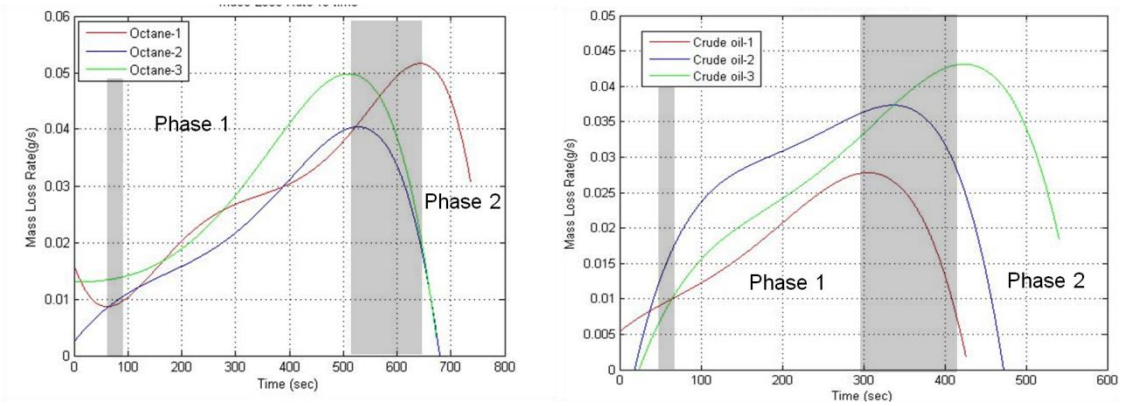

Fig. 13: Mass loss rate vs. time for octane (left) and ANS crude oil (right). Burning in an ice cavity, D = 5cm.

There are two phases observed for the burning behavior, first being the continuous increase to reach a peak and then a rapid decline to extinction. The two phases are

demarcated using the maximum mass loss rate. The first phase where the burning rate is found to grow steadily is caused by expansion of pool fire because of melting of ice. In this phase mass loss rate increases as liquid level rises (*U* decreases) and pool fire grows larger (*D* increases). This widening causes the fuel to stretch laterally by reducing its thickness at a faster rate. At some point, the fuel layer reaches a *critical* thickness where the losses outweigh the energy necessary to sufficiently vaporize the fuel thereby leading to extinction. At this point (start of Phase 2), the flame height decreases quickly and extinction is achieved. Experimentally it was observed that the critical fuel layer thickness approximately equals 0.7 mm for octane and 3 mm for crude. The result for crude is comparable with prior results reported in literature [4, 5]. On extinction the fuel was tried to be re-ignited using a butane torch; however, ignition was not possible (at least 3 attempts were tried).

Geometry changes

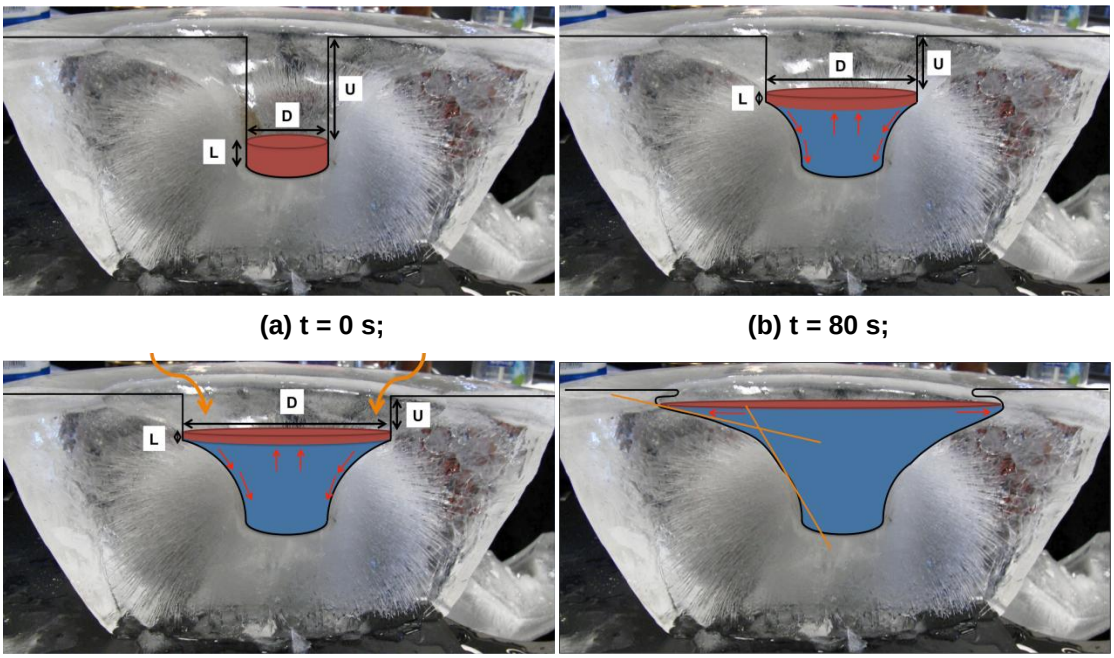

(a) t = 0 s; **(b) t = 80 s;**

(c) t = 150 s; **(d) t = 490 s;**

Fig. 14: Ice cavity evolution.

Figure 14 shows the evolution of a 5 cm diameter ice cavity schematically during the oil burn. The original ice cavity is cylindrical as shown in Fig. 14a. Water from the melting ice because of the heat transferred from the flame runs down to the bottom of cavity and causes the fuel layer to rise as shown in Fig.14b and c. An increase in diameter (*D* and reduction in ullage (*U*) enhances the burning and results in an increasing mass loss rate. Eventually, when the oil thickness reaches a critical value (2-3 mm) flame quenching is observed as shown in Fig. 14d. The slopes shown by two orange lines in Fig. 14d seem to indicate that the fuel layer tends to rise up to a certain ullage quickly and then at a critical ullage height starts expanding radially into the ice wall. This radial penetration was not expected and requires further experimental and theoretical analysis. However, it is clear that this radial expansion at a critical condition greatly influences the mass burning rate and efficiency. The implications of these phenomena are further discussed in Section 5, where large-scale test results are reported.

Two possible driving forces of flow inside the fuel layer are *natural* (driven by buoyancy forces) and *Marangoni* convection (driven by surface tension difference). Observations from the tests show an existence of strengthened Marangoni convection in the fuel layer especially close to extinction. More experiments are needed to examine the natural and Marangoni convection effects and their impact on geometry change.

The dynamic change of cavity and thickness of fuel layer were measured from frame by frame image analysis of a video camera. Figure 15a, shows the experimentally observed increase in the diameter (*D*) of the ice cavity for 5 cm and 10 cm trials. The final diameters of 5 cm and 10 cm trials are 13.5 cm and 17.5 cm, respectively. Figure 15 b, shows the thinning process of fuel layer because of the lateral expansion of the cavity. It is observed that regardless of the initial thickness the thinning process continues till the final thickness is reached (2-3 mm). As discussed, although the diameter is increasing causing an increase in burning rate there is also a consequent decrease in the fuel layer thickness. The resultant effect is a rapid deceleration of the mass loss rate as the fuel layer thickness surpasses its critical thickness for sustained combustion. At the critical thickness, conduction losses in the fuel layer are higher than the energy necessary for vaporization and sustained burning. Because of this reason, the flame quenches.

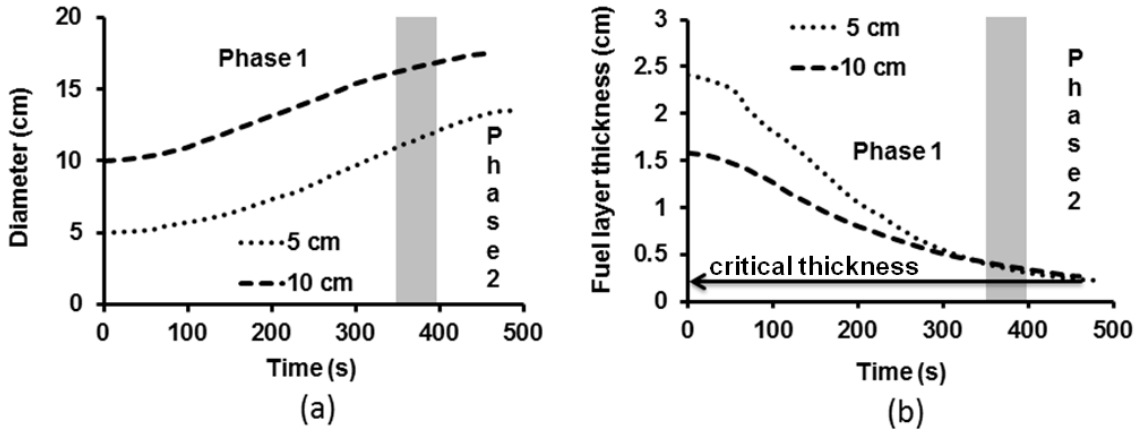

Fig. 15: a) Expansion of ice cavity in course of combustion. b) Fuel layer thickness decline. The arrow is marking the terminal fuel layer thickness.

Figure 16 shows expanding cavity for 5 cm (a) and 10 cm (b) trials in sequential time steps. Phase 1 and 2 are recognizable from these images as well. The first four images of each set show the increasing period of burning rate (phase 1) where the fire is growing in size and the last image with a characterized weak flame is representing the decay period (phase 2).

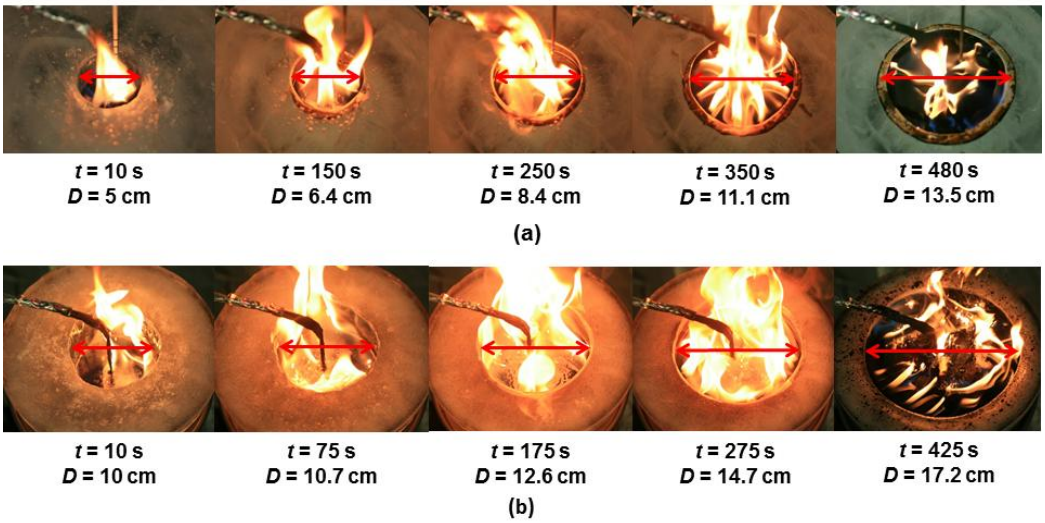

Fig. 16: Cavity expansion during burning in an ice cavity. (a) *D* = 5 cm and (b) *D* = 10 cm trial.

Figure 16 also shows the rising of the fuel layer as the cavity grows in size. As discussed earlier, the ice melting causes water accumulation inside the cavity causing the fuel layer to rise up. There exists a strong coupling between the geometry change (rate of ice melting) and the burning dynamics (rate of fuel vaporization, flame shape) which can be analyzed if the heat transfer processes are further explored. This is achieved by analyzing the temperature data.

Temperature profiles

Figures 17 and 18 show the temperature profiles along the centerline of octane and crude oil, respectively. This data was also used as a means of analyzing the movement of the fuel layer. It is observed (Fig. 17) there is an early increase in the 3 cm (C2) thermocouple temperature followed by a decrease. The early temperature increase is attributed to the low initial flame height while the rapid decrease is attributed to the melted water pushing the fuel layer above the thermocouple.

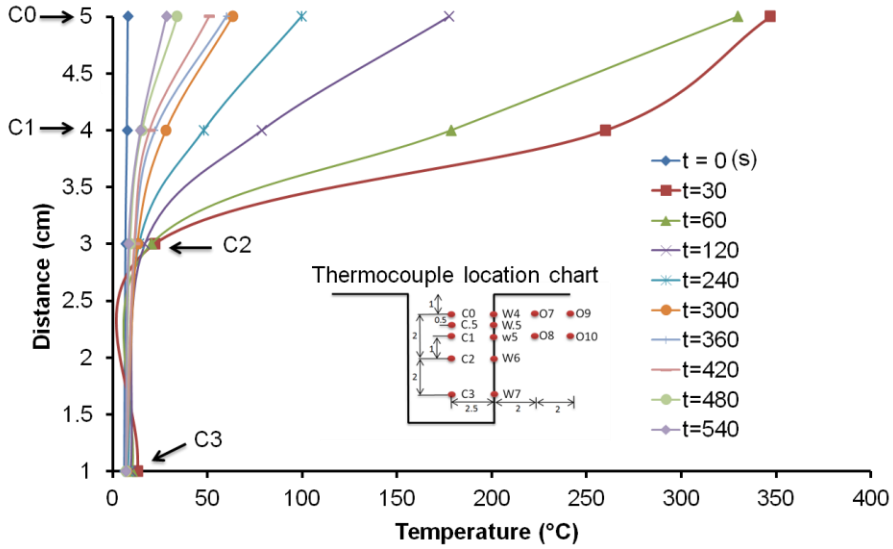

Fig. 17: In-depth temperature profile along the centerline for octane.

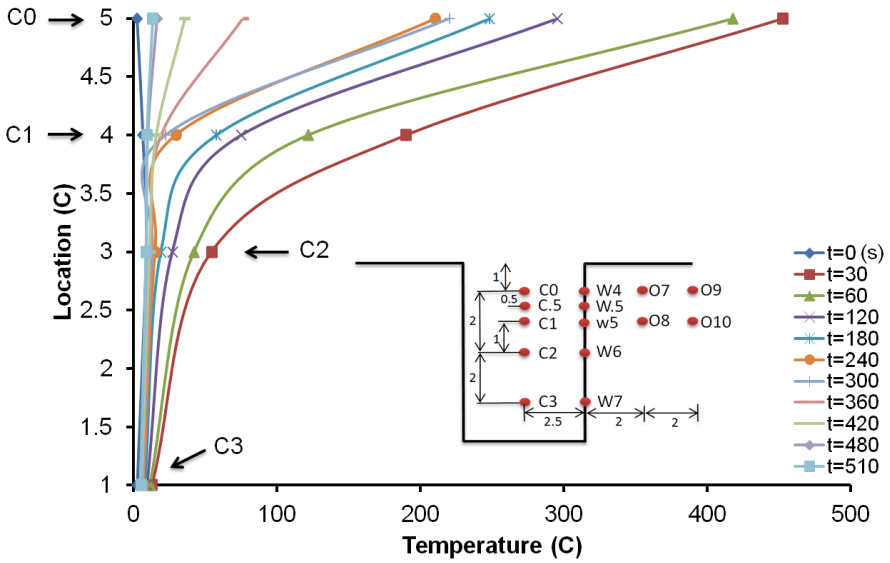

Fig. 18: In-depth temperature profile along the centerline for ANS crude oil.

At a point between the C0 and C1 thermocouple location the fuel layer no longer moves in the vertical direction but begins to move horizontally, penetrating the walls of the ice laterally. This movement corresponds to a stagnation of the temperature profile as shown in Fig. 17 and 18. These thermocouples reach a maximum temperature then systematically decline in unison until extinction; indicating a lack of vertical motion. The maximum temperature corresponds to the maximum mass loss rate and the formation of the ice lip. From the transition point the temperature of the liquid phase steadily declines as the critical thickness of the fuel layer is surpassed. The consistent behavior of the temperature profile between the 12 trials provides evidence to suggest that the point at which ice wall penetration occurs is independent of channel width. A similar trend is observed for the crude oil case shown in Fig. 18 as well. Further, the decreasing fuel layer thickness and penetration into the ice increase the conductive losses and prevents the fuel layer from achieving the necessary temperatures to volatize the heavier components of the oil. At the maximum temperature the gradient between the C0 and C1 thermocouple is nearly vertical providing evidence to suggest that the losses into the water layer are significant. As the trials progress through phase 2 the decreasing fuel layer thicknesses, increasing conductive losses, and fuel composition changes (for ANS crude oil) extinguish the flame.

To further explore the in-depth conduction losses from the fuel to the water layer, additional tests were performed where ice cavities with initial diameter of 5 and 10 cm were equipped with 16 thermocouples (TC) along the centerline as shown in Fig. 19. The increased number of TC's allowed systematic tracking of the fuel layer as it rises during the burning. The temperature data is also used as an input to the mathematical model discussed in Section 7.

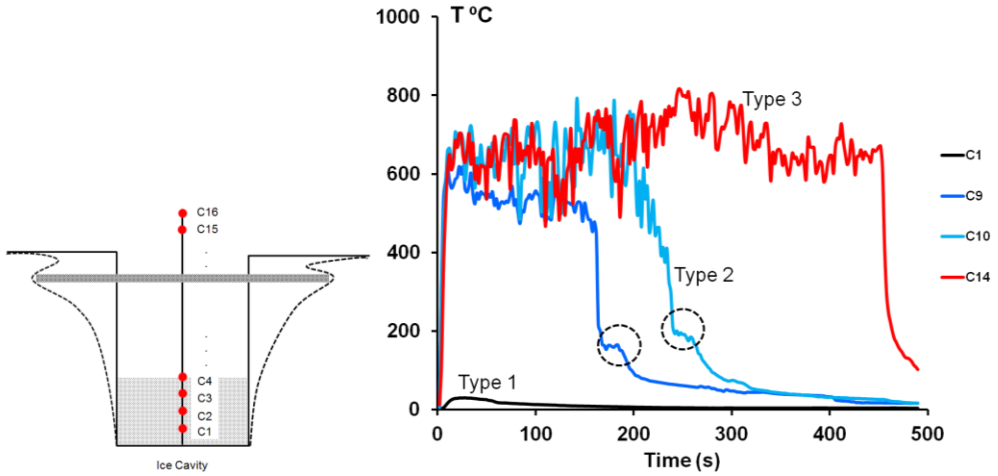

Fig.19: Sixteen thermocouple array arrangement to analyze in-depth conduction losses (left) and temperature data for D = 5 cm case showing 3 distinctive temperature trends (Type 1 – 3).

The temperature data showed three different trends as shown in Fig. 19 (right hand side). TCs located below the initial fuel layer record the temperature of liquid phase (first crude oil and then water). These are labeled Type 1 in Fig. 19. TCs between initial and final fuel layer location record the temperature of the gas phase initially and then after the elevation of the fuel layer they sink into the liquid phase. The temperature profiles collected using these TC's is labeled Type 2 in Fig. 19. Elevation of the liquid layer causes a sudden drop in temperature as indicated in Fig. 19 by the dashed circles temperature profiles from C9 and C10 labeled Type 2 and colored blue. The third group of TCs labeled Type 3 stays out of the liquid phase for the entire experiment and only record the gas phase temperature which is usually in the range of 600 – 800 ºC. Note that this does not indicate the flame temperature which is usually higher ~ 1500 ºC.

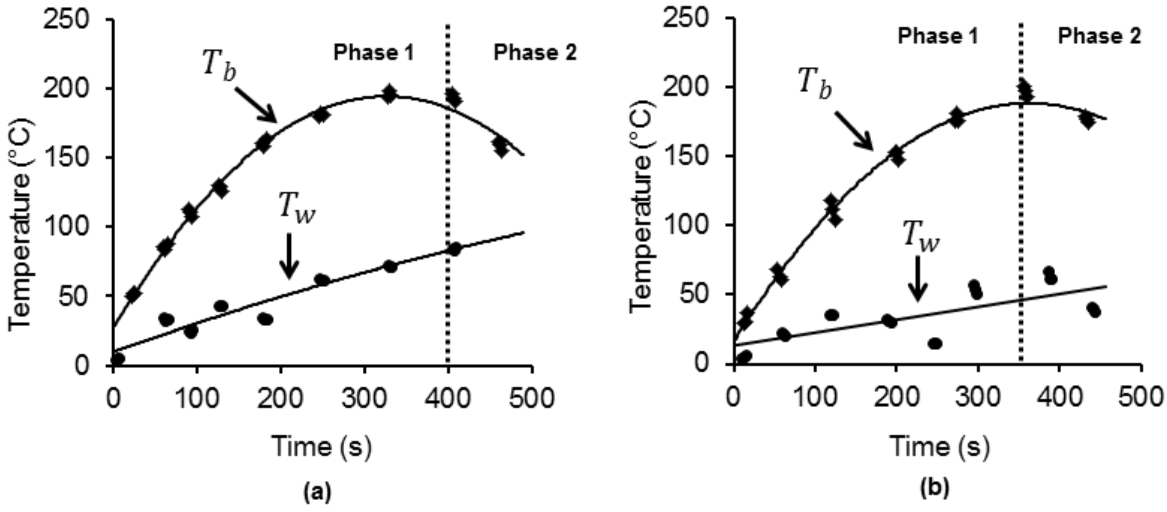

Fig. 20: Temperatures corresponding to top and bottom of fuel layer. a) D = 5 cm and b) D =10 cm.

The measurements from the Type 2 group of TCs are further analyzed to obtain the in-depth temperature gradient within the fuel layer. As shown in Fig. 19, a sudden drop of temperatures (~200 °C) for Type 2 group of TCs is identified in a time period shorter

than 5 seconds. This moment is defined as the point where the TC immerses into liquid phase. The measured temperatures of the TC for a period of 10 seconds after this moment are averaged and assumed to be the instantaneous surface temperature of crude oil denoted as T_b. Figure 20 shows the results obtained, where the surface temperature of fuel and the temperature of the water-fuel interface are plotted as a function of time. Similar to Fig. 13, Phase 1 and 2 burning regimes are also shown in Fig. 20 by dashed vertical lines. It is observed that the surface temperature of ANS crude generally increases in the first phase up until the burning enters the second phase. Declining temperature in Phase 2 also verifies the presence of a significant heat loss that halts the combustion process. Experimental data of fuel layer thickness vs. time from Fig. 15b enabled interpolation of the temperature reading of adjacent TCs to obtain the temperature of fuel and water interface. This trend is shown in Fig. 20 labeled as T_w.

3.4 Evaporation of liquid fuel because of externally applied heat flux

Figure 21 shows the experimental set up used to examine the change in geometry of the ice cavity with the addition of external heat flux. The basic idea was to separate or decouple the flame from the problem. In other words, the question of what would happen if a fuel in an ice cavity were exposed to a constant heat flux without the consequent burning is addressed using the experimental set up shown in Fig. 21.

Considering the changes in geometry of the ice cavity and its influence on the mass burning rate, it is important to understand if the change is because of the heat and mass transfer because of the heat flux from the flame or is it also dependent on the location of the flame with respect to the cavity. The ice block with a 5 cm circular cavity filled with fuel (ANS crude oil) is exposed to an external radiant heat flux from a conical heater. A cylindrical insulating cover placed on the top surface of the ice block (with the cavity exposed) is used to block the external heat flux to the ice. Thus, the external heat flux only impinges on the circular cavity. The insulating cover is made by a 1 cm thick water/oil 3M absorbent pad (for heat isolation and water absorbing), which is covered by a wrinkle-free aluminum foil. Heat fluxes of 30 kW/m^2 and 50 kW/m^2 were used to perform the tests. The dimensions of the cavity are similar to the tests reported in Table 4 for ANS crude (D = 5 cm, H = 6 cm). However, since oil was not ignited in these tests, the *critical ratio* does not apply in this case and tests were stopped when oil surfaces were about 0.5 cm away from the top surface of the ice. Similar to previous tests, visual data from cameras and a cross section of the ice-block after the completion of the test was used to interpret the experimental behavior.

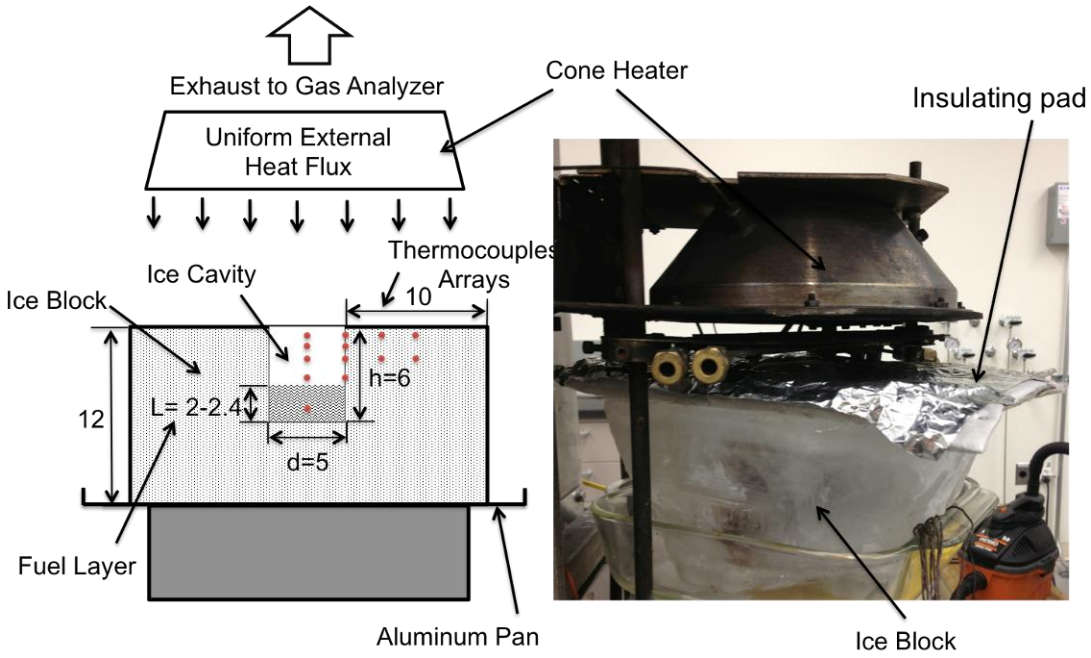

Fig. 21: Experimental setup with externally applied heat flux. ANS crude oil, no ignition.

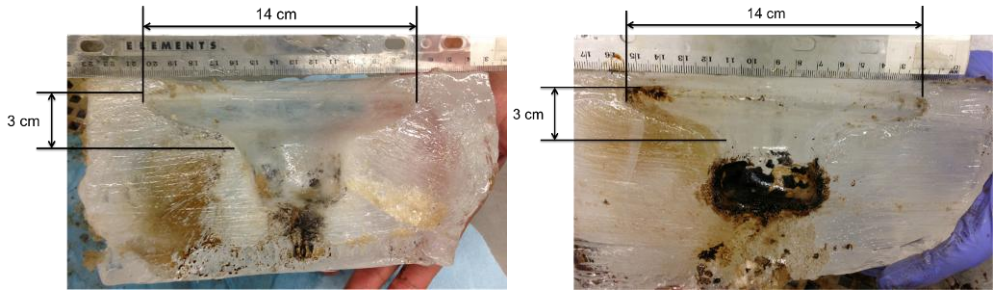

Fig. 22: Ice cavity geometry after exposure to radiant heat fluxes of 30 (left) and 50 kW/m^2 (right).

Figure 22 shows the geometry changes after the test. Interestingly the deformation produced is similar for both cases as shown in Fig. 22. In other words, increasing the heat flux does not increase the final size of the cavity. In both cases of external applied heat flux (30 kW/m^2 and 50 kW/m^2) the 5 cm outer edge of the cavity expands to 14 cm (180% increase), implying that the melting of ice within the cavity causing the overall geometry of the pool fire to change may be related to fuel characteristics (vaporization temperature, heat of gasification, viscosity) instead of the heat feedback of the flame.

4. Intermediate scale tests

4.1 Experimental results with octane in an ice channel

Three different channel sizes were chosen for this phase: 8(width) × 10(depth) × 30(length) cm^3, $12 \times 15 \times 20$ cm^3 and $8 \times 10 \times 65$ cm^3. The experimental set up is shown in Fig. 23. Based on the results of the small-scale tests (section 3.3), two parameters were the primary focus of the intermediate-scale tests; the first being the ratio of channel depth to channel width which to prevent overflow, and the second being the ratio of channel width to ice block width to maintain fuel containment. The former ratio was taken as 1.2 times the width while the later was taken as 4 times the channel width. From these factors both the ice channel dimensions and ice block dimensions for each trial were determined. Note that the parameters were obtained from small-scale tests using a 5 cm circular cavity and were successful in scaling-up to the intermediate scale. This is promising!

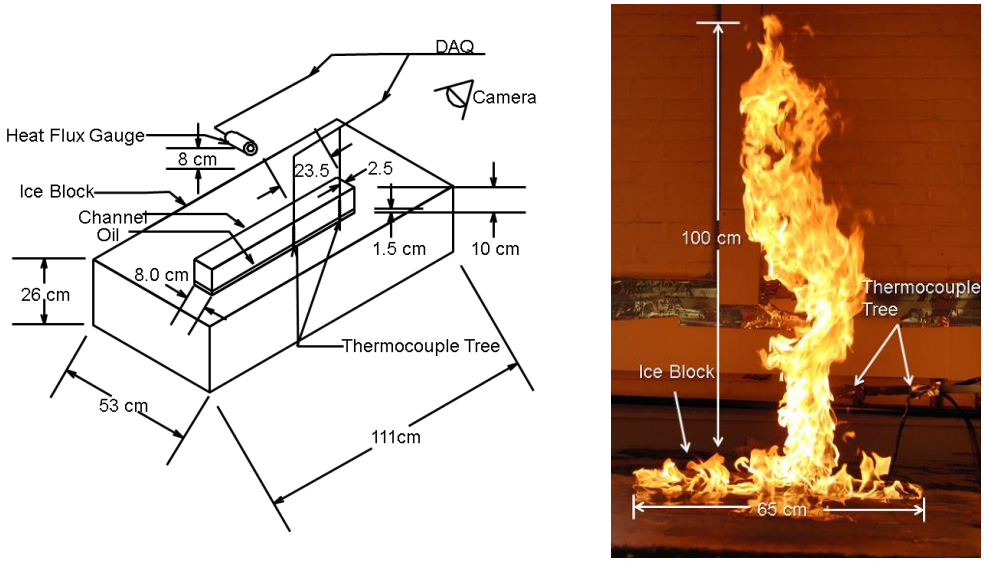

Fig. 23: The design on the left and picture of the flame during the intermediate scale on the right for 65 cm trial (octane).

Another important factor in preventing a breach of the ice channel is the depth of the fuel layer at the time of ignition. The fuel depth affects the duration of the trial which then affects the amount of ice that is converted to water. The 65 cm trial used 750 ml of octane or a 1.5 cm fuel depth. The trial lasted for approximately 11 minutes and corresponded to 6.5 L of melted ice, measured in the form of water. The photograph shown in Fig. 24 illustrates the dimensions of the ice cavity after burning was completed.

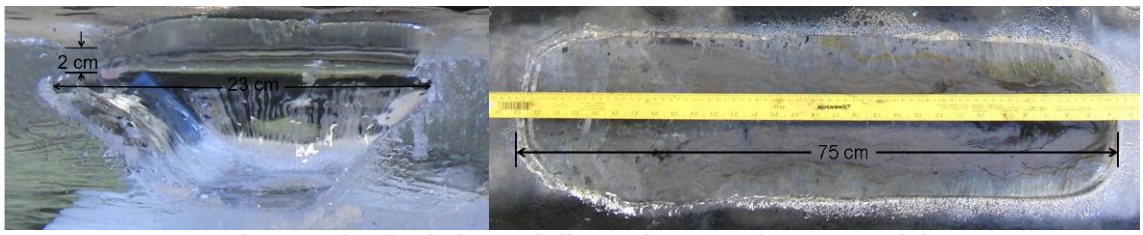

Fig. 24: The final channel dimensions for the 65 cm trial.

The final dimensions of the ice channel were 23 x 10 x 75 cm^3 which is a 330% increase from the starting condition. As shown in Fig. 24, the expansion of the channel was roughly 3 times the channel width, which was less than expected. The smaller expansion ratio may indicate that for the large-scale tests a smaller part of the ice will melt. No boil over was observed.

One of the more interesting observations was the ability to view the experiment through the ice block. Fig. 25 shows that it is possible to make out the water layer, fuel layer and flame when the ice block is sufficiently transparent. The transparency of ice depends on the formation process. It is possible to procure “clear’ ice as opposed to “carving” ice, although at an increased cost.

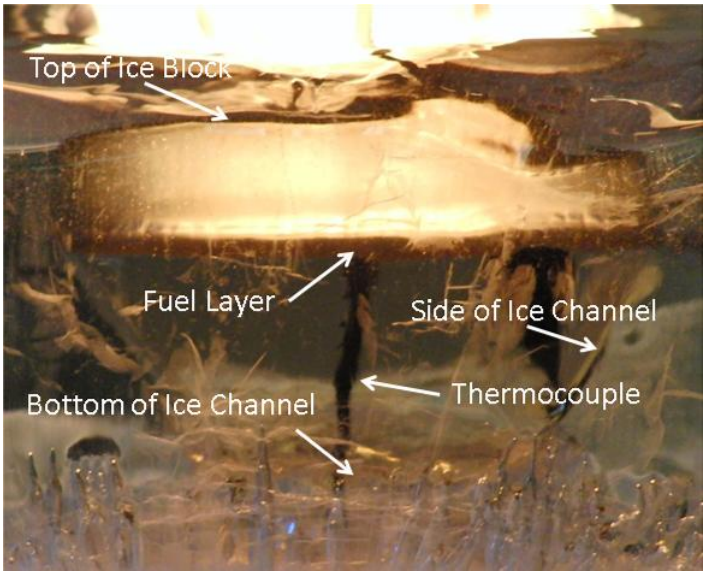

Fig. 25: Looking through ice at the fuel layer and ice channel boundaries are clearly visible.

4.2 Experimental results with ANS crude oil in an ice channel

Based on the results intermediate scale tests with octane, a channel size of 65(length) × 16(width) × 10(depth) cm^3 is chosen for the ANS crude oil burn for intermediate scale test. A 110 x 53 x 25 cm^3 ice block is used to carve out the channel. In this case, the *critical ratio* discussed earlier was further analyzed by varying the oil thickness. Three thicknesses of 0.5, 1 and 1.5 cm (Table 5) are chosen. Two repeated trials are conducted for each oil thickness. Figure 26a shows the experimental setup. Two thermocouple trees are placed at the center and adjacent to wall of the channel (Fig. 26). Each tree has 16 thermocouples spaced at 0.5 cm intervals. The spacing of the thermocouples on the tree is such that all of the measurements within the liquid phase are possible during all stages of the trial. The close spacing of the thermocouples allows for better resolution when measuring the rate-of-rise of the liquid layer. One heat flux gauge (labeled gauge #1 in Fig. 26a) is placed on the short edge of the ice block (55 cm away from the center of channel, 19 cm above the initial fuel surface). Three additional heat flux gauges are placed at the long edge of the ice block, which are 59 cm away from the center of channel and 39, 89 and 139 cm above the initial fuel surface.

Table 5: Three test cases with various oil thicknesses

Oil thickness (cm)	Total oil (g)
0.5	500
1	800
1.5	1275

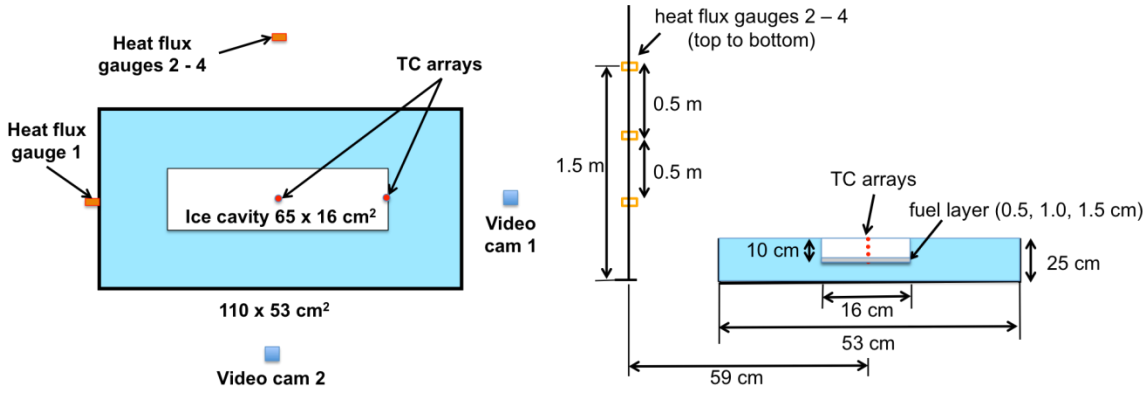

(a)

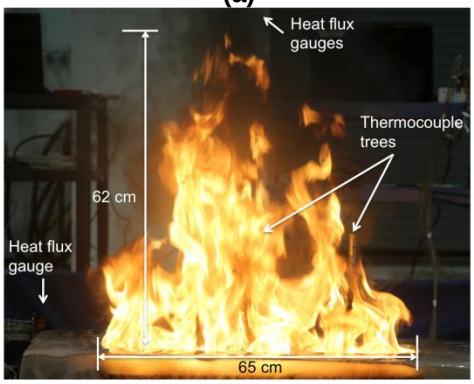

(b)

Fig. 26: Experimental set up (a) and ANS crude oil burn in 65 x 16 x 10 cm^3 ice channel (b).

Table 6 shows the average burning rates and burning efficiencies for 3 cases. Table 6 shows that the average burning rate increases as the initial oil layer thickness increases. The most likely reason for this behavior is because of the added widening of the cavity that can be caused because of increased quantity of oil. However, the same trend is not observed for the burning efficiency. The burning efficiency is highest (82%) for a case where the initial thickness of the oil layer is 1 cm and the *critical ratio (L/H)* equals 0.1. The burning efficiency decreases with an increase in the critical ration to 0.15, showing the influence of initial geometry of an ice cavity. The controlling parameters related to the difference in trend between the average mass burning rate and burning efficiency need to be further analyzed. Also note that at the intermediate scale, boilover occurs in all tests. Table 6 shows the average time to boilover and time to extinction for each case. Burning is enhanced due to boilover and both burning rate and burning efficiency are thus increased.

Table 6: Burning behavior comparison of 0.5, 1.0 and 1.5 cm thickness oil burn

Oil thickness (cm)	Critical ratio (*L/H*)	Total oil (g)	Residual (g)	$t_{boilover}$ (s)	$t_{extinct}$ (s)	MLR/area (g/s-cm^2)	Burn efficiency
0.5	0.05	503	174	140	198	0.0016	66%
1	0.1	808	147	210	280	0.0023	82%
1.5	0.15	1274	297	240	315	0.0030	77%

The ice cavity geometry change is also investigated for 3 cases and shown in Fig. 27. All 3 cases have the same initial ice channel dimension, but with increased initial oil thickness, greater expansion of the channel is observed. Channel width increases from 16 cm to 27 cm for 0.5 cm initial oil thickness, from 16 cm to 29 cm for 1 cm and from 16 cm to 33 cm for the 1.5 cm initial thickness case. The burning area is increased as initial oil thickness increases and as mentioned previously is the most likely reason for an increase in the average burning rate with increasing initial thickness of oil. As burning continues the melted water fills the cavity causing the oil layer to rise up. This rise is highest for the 1.5 cm thick oil layer. The result is that a thinner ice "lip" (2 cm) is formed compared to a 5.5 cm thicker ice "lip" formation in 0.5 cm case. The final dimensions of the ice cavities after the burn are shown in Fig. 27. The smaller ullage for the thicker oil layers could also cause a higher average burning rate since it allows more air is entrainment to support combustion.

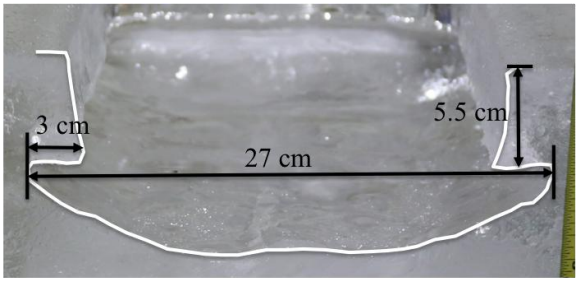

Fuel thickness: 0.5 cm

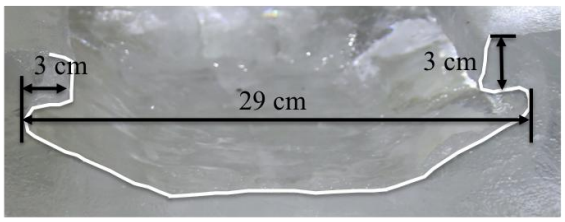

Fuel thickness: 1.0 cm

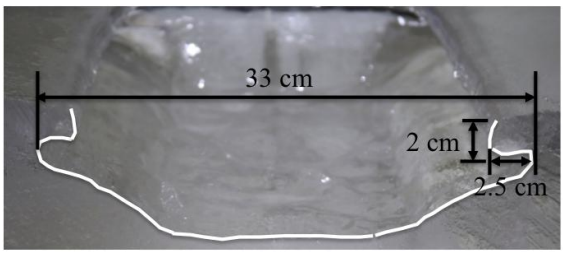

Fuel thickness: 1.5 cm

Fig. 27: Final channel dimensions for 0.5, 1.0 and 1.5 cm initial oil thickness trials in 65 x 16 x 10 cm^3 channel.

The lateral penetration below the ice “lip” for all 3 cases is similar (2.5 - 3 cm). This indicates that the oil penetration underneath the “lip” is most likely not a function of the initial oil thickness. However, the experimental results are not conclusive to verify this exactly and further experiments are necessary to thoroughly investigate the lateral cavity formation. From a practical standpoint the lateral cavity formed during the burning masks the crude oil trapped within from flame heat flux. This may reduce efficiency.

Flame heat flux

Flame heights during the oil burn are shown Fig. 28 for 1.5 cm initial oil thickness case at different time intervals during the burn. It is observed that approximately 50 s after burning reaches a quasi-steady sate until boil over at t = 240 s. The flame height and also the flame heat flux reach a maximum value at t = 280 sec. Extinction is observed at t = 314 s. It is observed that extinction is rather sudden similar to small-scale tests (Phase 2) discussed in section 3.3

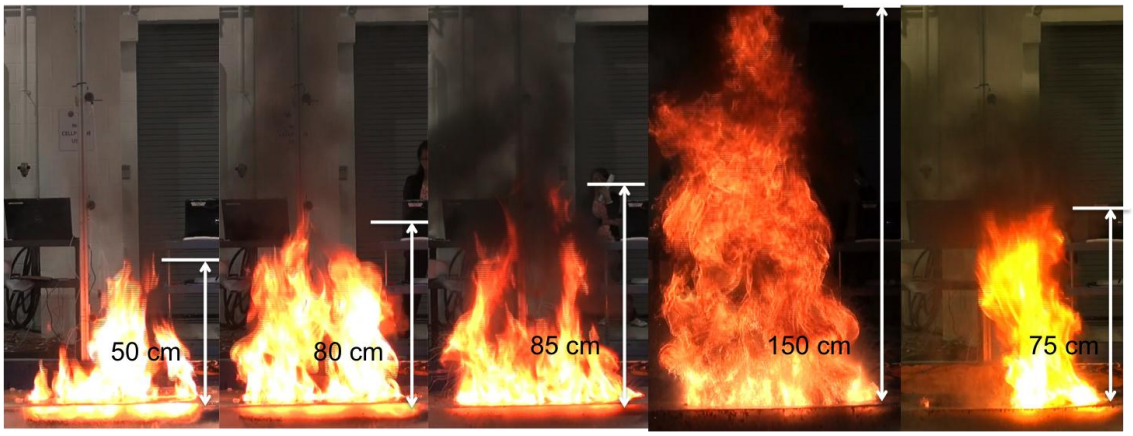

Fig. 28: Progression of the intermediate scale experimental trial (1.5 cm initial oil thickness, ANS crude oil. 65 x 16 x 10 cm^3 channel).

The radiative heat fluxes at 2 locations are shown in Fig. 29. Figures on the left show the radiative heat flux measured at 55 cm (22 cm from the pool short edge) and figures on the right show the maximum radiative heat flux measured at 59 cm (51 cm from the pool long edge) from the pool center (locations as shown in Fig. 26).

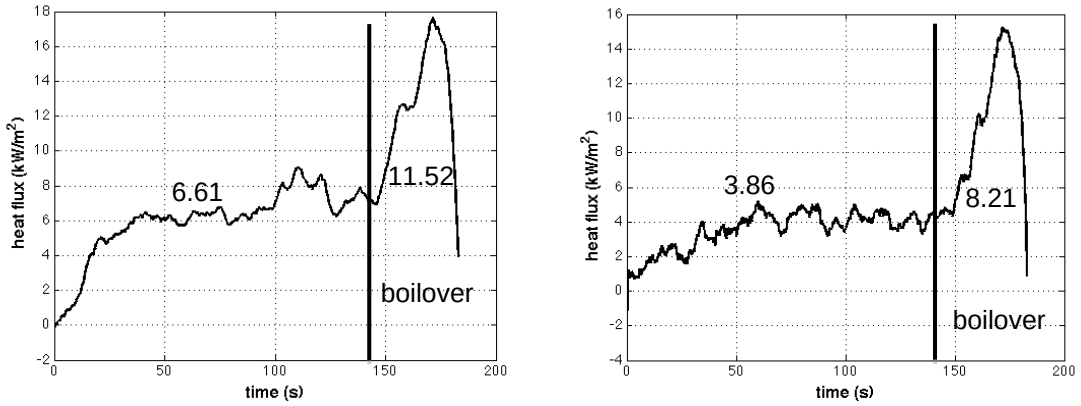

(a) 0.5 cm oil thickness

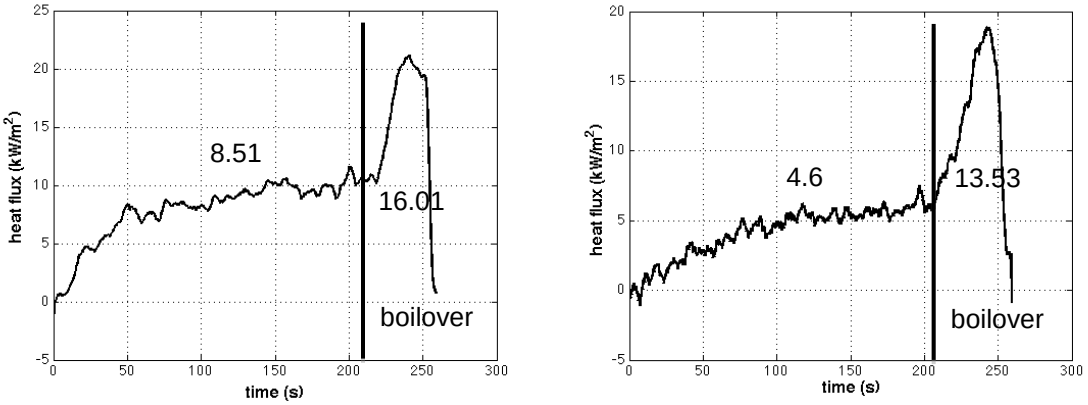

(b) 1.0 cm oil thickness

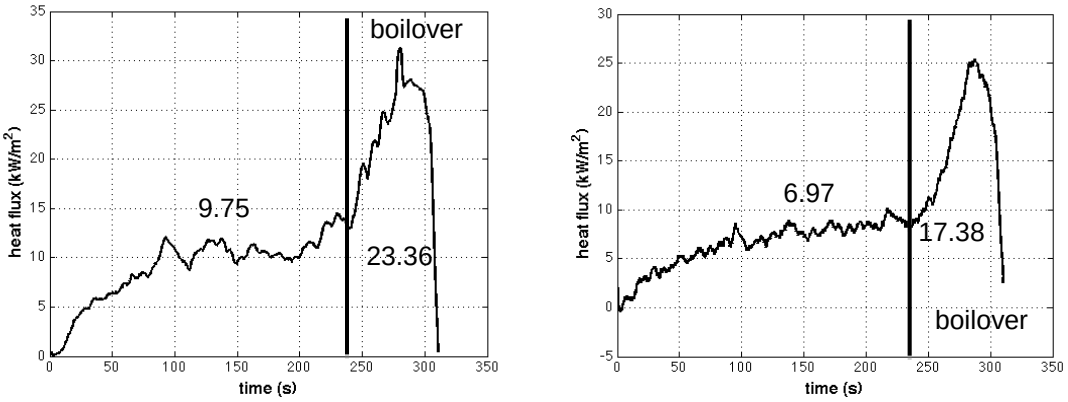

(c) 1.5 cm oil thickness

Fig. 29: Radiative heat fluxes measured for 3 experimental trials with ANS crude oil at intermediate scale.

Since the radiative heat flux is enhanced significantly during the boil over period, time to boil over is marked on each plot. The average radiative heat fluxes for pre-boilover and boil over period are also marked on the plots. It is observed that as the initial oil thickness increases, the radiative heat flux from the flame also increases. This is in accordance with the increase in average burning rate observed with increasing fuel thickness. Also note that Fig. 29c shows maximum radiative heat flux at 280 s corresponding to the maximum observed flame height.

5. Experimental results and discussion for test at the large scale (~1 m)

Large-scale tests were conducted at the new fire laboratory (area of 240 m^2) at WPI shown in Fig. 30. The capacity of the large hood is 60,000 ft^3/min (28 m^3/s) and can handle a 3MW steady state fire. The hood is 6 × 6 m^2 and is 5.5 m above the floor. The dock is 0.9 ×1.5 m^2. A test area of 6 x 6 m^2 is achievable for testing. Based on the small-scale and intermediate scale experiments, given a 1.5 cm fuel depth, the pool's final surface area increase 2 times; which suggests that for a 1 x 1 m cavity 3 x 3 m^2 ice containment is required.

Fig. 30: WPI-facility for large-scale test

Figure 31 shows the experimental setup for the large-scale test. The design consists of a 3 m (L) x 3 m (W) x 0.3 m (H) outer frame made of plywood wrapped by two 5 m x 6 m fire-resistant and waterproof sheets. An array of carving ice blocks, each 1 x 0.5 x 0.25 m^3 (actual size varies), are placed around the perimeter of the container leaving a 1.09 x 1.17 m^2 area at the center. Ice blocks are fused together to prevent the oil from spreading into the gaps. A thin layer of water (2.5 – 3 cm) is added into the cavity as a base to prevent the oil from spreading underneath the ice blocks.

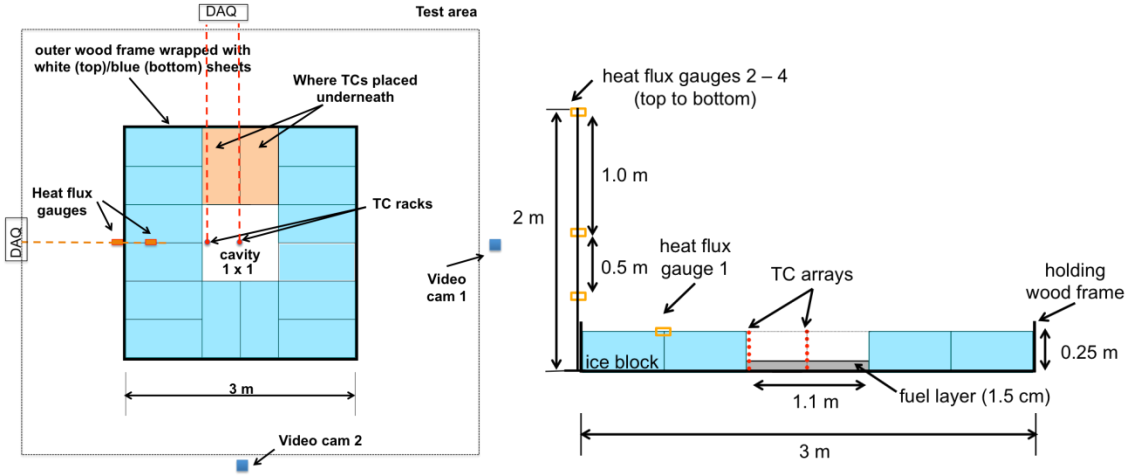

Fig. 31: Experimental setup for large-scale test.

Two thermocouple trees (at the center of the cavity and adjacent to the wall) are spaced around the fuel layer to measure the temperature distribution and record the movement of the liquid layer. One heat flux gauge (HFG 1) is placed on the top surface of the ice, which is 0.75 m away from the center of the ice cavity to measure the heat flux reaches the ice surface from the flame. 3 additional heat flux gauges are placed 1.5 m away from the center of the ice cavity and 0.5, 1.0 and 2.0 m above the ground (HFG 4, 3, 2) to measure the radiant heat flux from the flame. Two video cameras are used to record the burning process: one was placed horizontally; another is placed 4 m above the ground (outside of test area) on a platform built for servicing the large hood. This camera provided an aerial view of the entire test. 9.8 kg of ANS crude oil is poured into the ice cavity to form a 1.5 cm thick oil layer above the water base as shown in Fig. 32. Note that the quantity of oil is nearly 8 times that used in the intermediate scale tests. The oil container was refiregerated such that initial crude oil temperature was ~2 ºC. Details of the experimental plan and procedure for the large-scale test are provided in Appendix D.

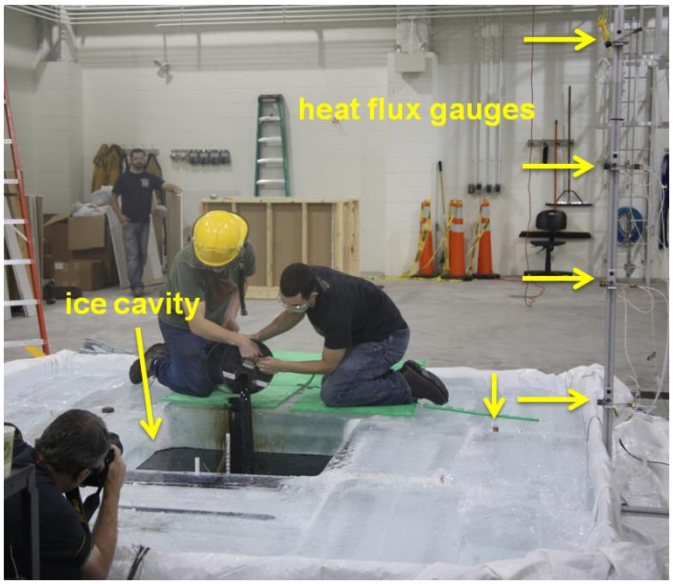

Fig. 32: Pouring ANS crude oil in the ice cavity (1.1 m^2 and 0.16 m deep). Crude oil mass = 9.8 kg, thickness in cavity = 1.5 cm.

The oil is ignited by a butane torch with an extended arm. The burn lasts for 197 seconds and extinguishes naturally. The oil does not flow out of the cavity since it is well below the critical ratio identified in the small-scale tests. L/H = 0.06 for the large-scale test and L/H_{crit} = 0.4 for ANS crude). After extinction, the remaining oil (heavy component residue) is collected by 3M oil only absorbent pads. The absorbent pads were weighed before and after the clean up to obtain 1.6 kg oil that remained postburn giving a burning efficiency of ~ 85%. Note that the burning efficiency is higher than the small and intermediate scale tests. The average mass loss rate per area is 0.0032 g/cm^2-s. This corresponds to a regression rate of roughly 2.5 mm/min.

Similar to the intermediate scale tests, boil over is also observed in the large-scale test. About 80 seconds after ignition, a transition to boil over is visually observed. The burning is enhanced after 100 seconds (after ignition) when it is in the boil over regime, as shown in Fig. 33. Temperature data from 2 thermocouple trees show that the heat flux from the flame was high enough to cause both supporting frames of the thermocouple trees to melt at 100 seconds. Luckily, only the top half of the center thermocouple tree

was damaged due to the high heat flux in the boilover period. The temperature profile in the fuel/water layer was still captured and is presented later.

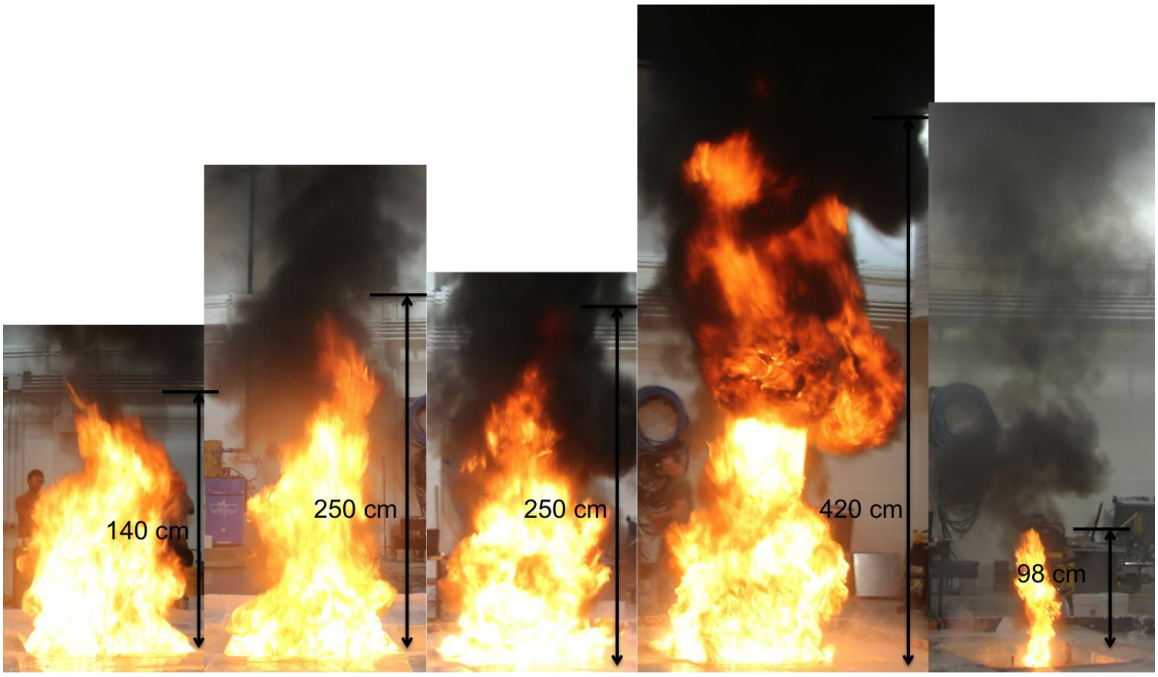

Fig. 33: Flame height at different time steps.

Table 7 shows the flame heights at various time steps and the corresponding heat release rates from the 1.1 x 1.1 m^2 crude oil pool fire (1.28 m of effective diameter), which are calculated using Heskestad's [6] correlation:

$$L_f = 0.23\dot{Q}^{2/5} - 1.02D, \qquad (1)$$

where L_f is the flame height, $\dot{Q}$ is the heat release rate and D is the pool diameter. Flame heights at different time steps during the large-scale test were measured using the video camera and corresponding heat release rates using Eq. 1 are shown in Table 7. It is observed that the most intense burning occurs 148 s after the ignition when the flame height was 4.23 m and the heat release rate reached 2842 kW. This is an impressive fire size, especially for a sooting fuel as shown in Fig. 33.

Table 7: Heat release rates for 1.1 x 1.1 m^2 pool

t (s)	L_f (m)	Q (kW)
1	0.18	106
13	1.41	479
23	2.41	1049
49	2.50	1114
65	3.08	1588
127	2.75	1306
138	3.60	2101
148	4.23	2842
157	3.96	2508
171	2.90	1430
194	2.30	973
198	0.98	311

Radiative heat flux from the flame to the enviroment was measured by a set of water cooled wide angle (150°) heat flux gauges (Medtherm 64 series) at various vertical positions above the initial fuel surface and various distances *L* of 0.75 m (in ice) and 1.5 m (outside of ice) from the pool center. The heat flux located at 0.75 m, was installed inside the ice surface facing up. Radiative heat fluxes measured by 4 gauges are shown in Fig. 34. Time of boilover and the average heat fluxes in pre-boilover and boilover period are also shown in Fig. 34 a-d.

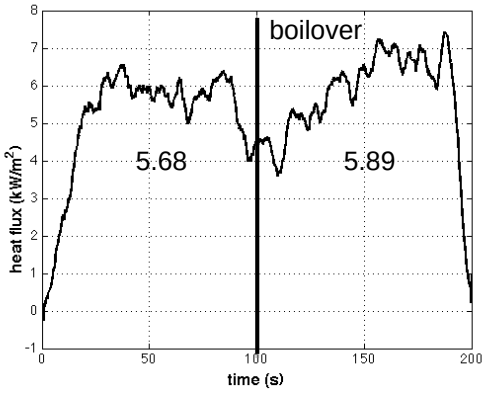

(a) HFG 1

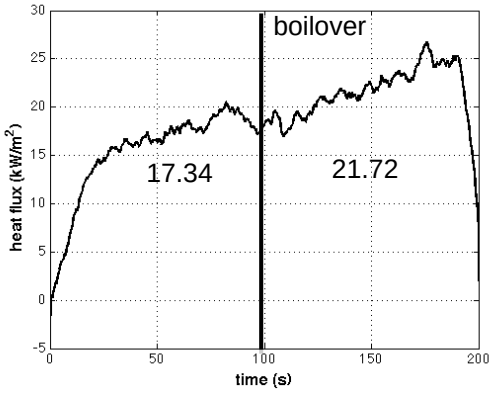

(b) HFG 2

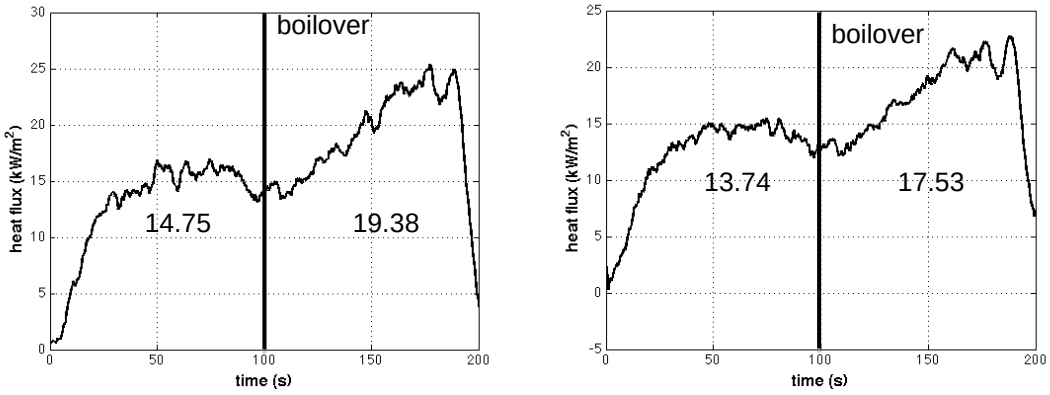

(c) HFG 3 **(d) HFG 4**

Fig. 34: Radiative heat flux measured using the heat flux guages.

As shown in Fig. 34, the radiative flux received on the ice surface (0.2 m above the initial fuel surface and 0.75 m away from the pool centerline) was only about 1/3 of the radiative flux received at the location of 1.5 m away from the pool centerline. The radiative heat flux from the flame thus has a tendency to radiate outwards rather than back to the ice surface. This causes significantly less ice to melt away in the large-scale test compared with the intermediate and small-scale tests. The rise of the fuel layer upwards because of melting of ice and corresponding water collection in the cavity is only 4 cm as shown in Fig. 36. This is significantly smaller than the small and intermediate scale test results. Because of less melting of the ice, the fuel layer does not rise as rapidly as in the small-scale tests. The significantly less flow of water into the cavity may also be the reason for early boil over. In the small-scale tests, there is a continuous supply of water from melting ice walls. The cold water keeps the water sublayer (layer of water below the oil) cool thereby not causing boil over. This trend is not observed in the intermediate and large-scale tests. Another reason for the low heat flux reaching the ice surface may be because of the strong convective air current parallel to the ice. For a large fire, air entrainment into the ice cavity along the top surface of the ice is cooled because of the ice. The heat flux emitted from the flame to the ice top surface is lowered by the entrained “cold” air.

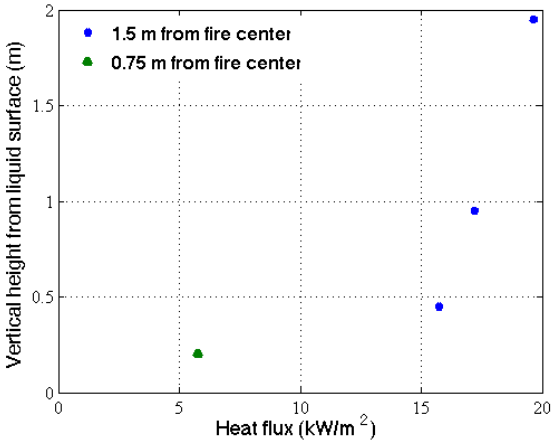

Fig. 35: Radiative flux distributions in a vertical plane at distances 0.75 and 1.5 m from 1.1 m x 1.1 m crude oil pool centerline.

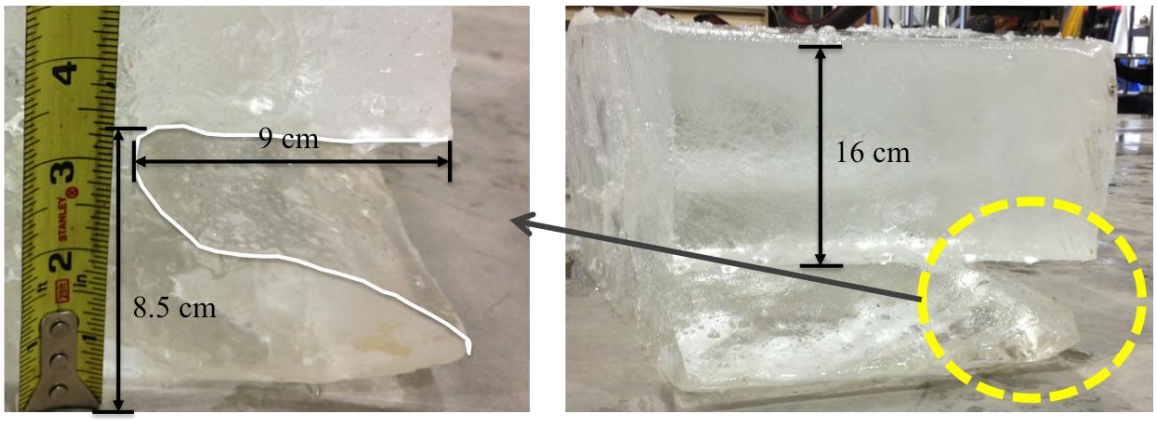

Fig. 36: Final dimension of large-scale test.

The radiative energy emitted from the flame is estimated using the the radiative heat loss fraction χ_R is defined as [7]:

$$\chi_R = \dot{Q}_R / \dot{Q}, \qquad (2)$$

where $\dot{Q}_R$ is the total radiative energy emitted from the flame and $\dot{Q}$ is the total heat released by the flame. Assuming the radiative energy to be isotropic

$$\dot{Q}_R = 4\pi L^2 \dot{Q}'', \qquad (3)$$

where $\dot{Q}''$ is the data captured by the heat flux gauges located at distance *L*. The total heat release rate from the flame was obtained by

$$\dot{Q} = \dot{m} \cdot \Delta H_C, \qquad (4)$$

where $\dot{m}$ is the measured mass loss rate (41.62 g/s) and ΔH_C is the heat of combustion of the crude oil (44.77 kJ/g @ 25°C), assuming the combustion is complete. Using Eq. 2 - 4 the average radiative fraction χ_R equals 0.27. This is in agreement with hydrocarbon pool fires of ~1 m diameter size range.

Temperature profiles

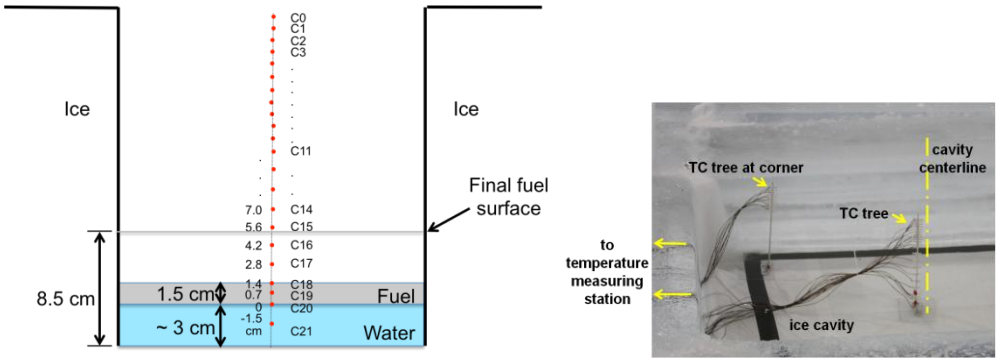

Fig. 37: Thermocouple distribution along pool centerline.

Figure 37 shows the thermocouple distribution along the pool centerline that was used in the large-scale test. The thermocouple tree was specially prepared using K-type TC's for

the tests. Thermocouples C0 – C21 were supported by a 27 cm long metal rod that was bolted to an acrylic base. It comprised of a metal rod bounded by insulation tape to which 22 TC's were systematically bounded using thermocouple cement. Individual TC's were threaded through a ceramic tube with only the bead exposed (about 5 mm of the TC wire and bead was exposed). Individual ceramic rods provided structural integrity during the test. Thermocouple wires were bounded by wire straps, and passed underneath the ice blocks to a temperature measuring station located 5 m away from the pool centerline.

During the test, 3 thermocouples (C18 – 20) were originally in the fuel layer, where C20 was initially located at the fuel/water interface. C21 was always inside of the water sublayer shown by blue in Fig. 37. All other thermocouples were initially above the fuel surface. As the oil burns, water from the melting ice accumulates at the bottom of cavity and fuel layer rises. The final fuel surface is experimentally determined as between thermocouple C15 and C16, as shown in Fig. 37.

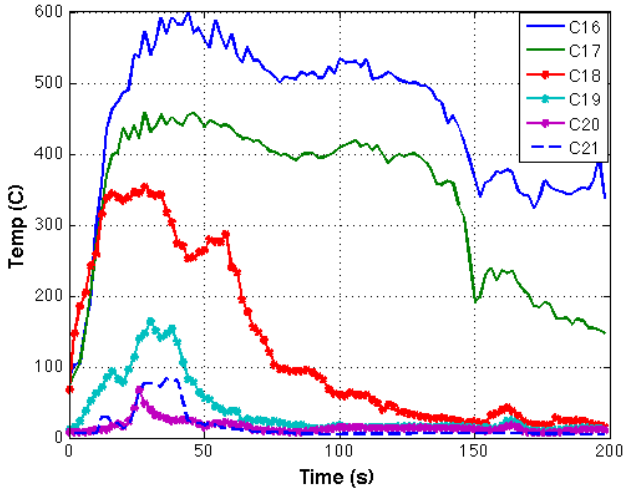

(a) Temperature vs. time

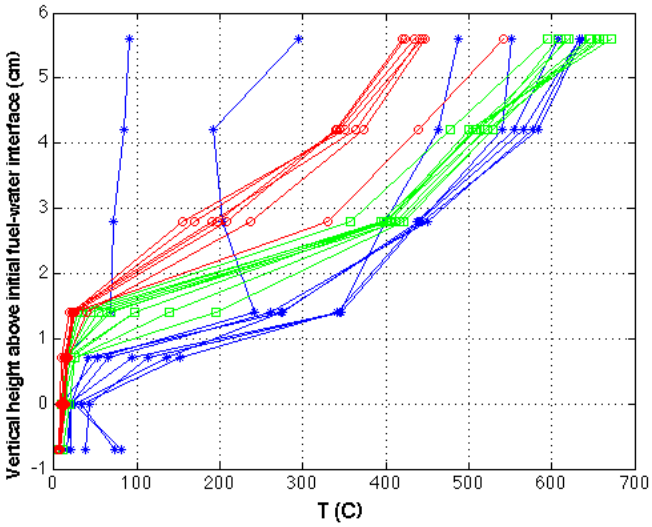

(b) Temperature vs. vertical height above initial fuel/water interface at time steps (Δt = 8 s);

(Blue star: 0-60 sec, green square: 61-140 s, red circle: 141-197 s.)

Fig. 38: Thermocouple distribution along pool centerline.

Figure 38 shows temperature profiles of thermocouple C16 - C21 as a function of the time (a) and as a function of the vertical height above the initial fuel/water surface at different time steps (b). From Fig. 38a and b, one can see that C16 could be immersed in the fuel or boiling fuel/water mixture (due to boil over) after 150 sec of ignition. C21 was always in the water, its temperature never went over 100°C. C20 was originally at the fuel-water interface and then immersed into the water after about 25 sec as ice melted and water accumulated into the cavity bottom. As more water accumulated inside the cavity, C19 is immersed into water after about 45 sec. C18 was initially at the fuel-air interface and as the fuel layer rose up, it was in the vapor, then into the boiling layer and eventually immersed into water after 75 sec. Oil reached at C17 after about 140 sec and after that, C17 might be immersed into a hot boiling water layer eventually.

As discussed earlier, the water from melting ice wasn't as much as what we observed from the tests in small-scale and intermediate scale. The overall cavity size expanded by only 3% compared with 150% in the small-scale and about 50-70% in the intermediate scale tests. The reason for this trend needs to be further investigated by performing a few more tests at the large-scale with different *L/H* ratios. However, it is interesting to note that the lateral cavity of approximately 0.1 m thickness is formed in the large-scale tests as well. This corresponds to about 12% of the fuel which is "trapped" and nonrecoverable. To achieve a reasonable efficiency in an ice cavity therefore warrants further work in understanding the controlling parameters associated with the lateral ice-cavity formation.

6. Comparison of burning at different scales

6.1 Average burning rate

As discussed previously, it was not possible to measure mass loss rate as a function of time for larger diameter cavities because of experimental limits with the load cell capacity. The initial and final mass of fuel and time to burning was used to obtain the average mass loss rate and burning efficiency. The average mass burning rate per unit area divided by the density of ANS crude gives the average regression rate which is usually used to represent the burning behavior of liquid pool fires [8]. A similar approach was used to present current experimental data as well.

Figure 39 shows the average regression rate plotted as a function of diameter (initial diameter of ice cavity is used) for all tests performed by WPI in this study with ANS crude oil. Experimental data points are highlighted with pink, blue and orange dashed squares to indicate small, intermediate and large-scale test data. Experimental data from other studies such as Blinov and Khudiakov [9]; Hall [10]; Gottuk and White [8] are also shown for comparison. Note that the previous experimental data represents average regression rate for confined pool fires; usually fuel contained in a metal vessel of diameter *D (m)*. Similar tests were also performed by WPI for ANS crude oil used in the study. The blue circles and corresponding blue experimental trend-line show baseline tests of ANS crude oil burning in 3.5, 10, 14.2 and 55 cm diameter steel pans. The baseline data shows similar trend and the same order of the magnitude as the petroleum curve (data from Hall[11]).

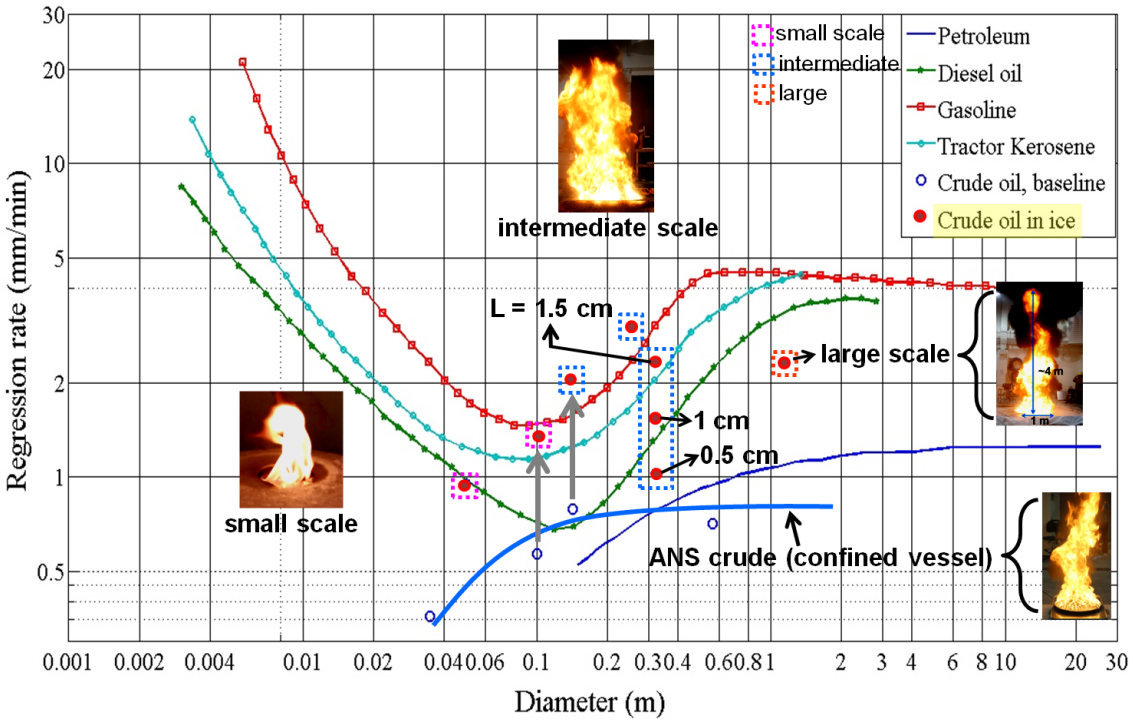

Fig. 39: Average regression rate

Figure 39 shows that the regression rate starts high (for small pools ~ 1 cm) and then decreases for sizes of 10 -15 cm. After this it increases once again and reaches a constant value at a size of 100 cm or 1 m as shown in Fig. 44. This large-scale constant regression rate for large pool fires is in the range of 1 to 5 mm/min. This range is also

comparable for large-scale oil-slick fires in the ocean as shown by Evans et al.[12] where a series of 14 experiments ranging from 0.4 to 17 m were conducted and the burning rate as indicated by the regression of the oil surface was ~3.3 mm/min. It can be said that the trends shown in Fig. 39 are applicable for a wide range of fuel types and differences in magnitude are mostly due the chemical composition of the fuel.

What's new and different with ice?

The results of current experiments in ice cavities of initial diameter *D* are shown with a red circular symbol. In general, the average regression rate of ANS crude burning in an ice cavity increases by 3 times that of a similar sized confined vessel. Two upward pointing gray arrows (Fig. 39) show a one to one comparison for small and intermediate sized tests where the regression rate of ANS crude burning in a steel pan (blue circle) is about 3 times lower than the corresponding burn in an ice cavity. This is because the surface area of the cavity increases as the ice melts during the oil burn. Although ice melting and consequent lateral expansion causes layer thinning, the influence of an increase in diameter seems to be a more dominant effect. A similar result was also shown by Bellino et al. [13]. For the intermediate and large-scale tests, it was also observed that this water sublayer eventually causes boil over, which further enhances the burning rate.

As shown in Fig. 39 an interesting behavior is observed for the intermediate scale tests with an ice cavity (effective *D* ~ 36 cm) where different initial oil thicknesses were used. The 3 data points (from bottom to top) are for trials with oil thicknesses of 0.5, 1.0 and 1.5 cm forming three different critical ratio's (*L/H* = 0.05, 0.1, 0.15 respectively). As shown in Fig. 39, for the same initial diameter, the average regression rate increases with an increase in the critical ratio. The results show that for field application of ISB in the Arctic, besides fuel layer thickness, the geometry of the cavity (*L/H* ratio) also plays a significant role.

6.2 Burning efficiency

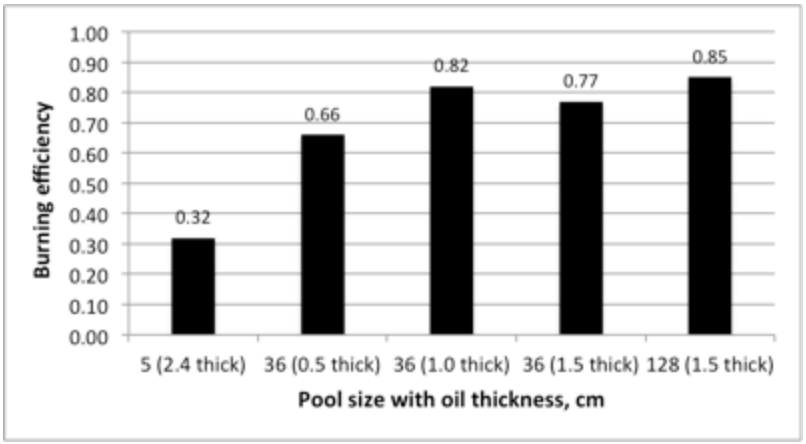

Fig. 40: Burning efficiencies of 5 test trials.

The burning efficiencies of the ANS crude oil burn at 3 scales are shown in Fig. 40. When initial ice cavity size increases, the burning efficiency increases also. Meanwhile, when the initial fuel layer thickness increases, the burning efficiency also increases. For the same oil thickness of 1.5 cm, burning efficiency for initial cavity diameter of 36 cm (intermediate scale) and 128 cm (large scale) could reach 78 - 85%. This is mainly due to boil over. For the baseline tests (under ambient condition), which are tests carried out in steel pans (confined pool fire) with ANS crude oil, the burning efficiency was more

than 90% for 10, 14.2 and 55 cm diameter pools and was only 46% for 5 cm diameter pool. Boil over was not observed in this case because no water sublayer was present when burning in steel vessels. The baseline test data is reported in Appendix C.

6.3 Geometry change

The geometry change of the ice-cavity affects the oil burning rate. Figure 41 shows the geometry change before and after the burn, separately, for the 3 scales (small, intermediate and large). It is observed that the 5 cm ice cavity had the largest surface diameter change (original/final diameter ratio, 0.38) after the burn and the 128 cm pool had the smallest surface diameter change (large original/final diameter ratio, 0.97). The results are summarized in Table 8.

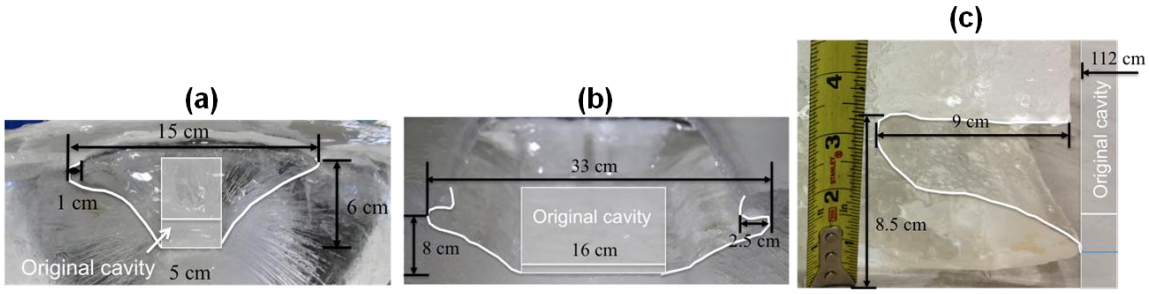

Fig. 41: Cross section of the ice cavity after each burn: (a) small-scale; (b) intermediate scale (1.5 cm oil thickness); (c) large-scale.

Figure 41 shows the original cavity cross sections as rectangular light gray shaded region, with the original fuel surface location by a horizontal line. The geometry after the burn got by cutting the ice cavity transversely after the experiment is also shown. The formation of the lateral cavity (similar to that observed in Bellino et al. [13]), where the oil tends to dig sideways into the ice thereby forming an ice-lip is clearly observed for the three cases as shown in Fig. 41 a, b and c. It is observed that the ice-lip increases in size from small, intermediate to large-scale.

Table 8: Heat release rate, burn efficiency and ice cavity dimension change for all 3 scales

Ice cavity D (cm)	Fuel thickness (cm)	D/D_final*	HRR (kW)	Burn efficiency	Unrecoverable oil fraction
5 (small)	2.4	0.38	1.16	32%	18.7%
36* (intermediate)	0.5	0.82	74.32	66%	35.2%
	1.0	0.77	105.66	82%	17.6%
	1.5	0.71	138.79	77%	11.7%
128* (large)	1.5	0.97	1863.33	85%	11.4%

* Effective diameter of noncircular ice channel.

The width of the lip width equals 1, 2.5 and 9 cm for tests in small, intermediate and large scales. The existence of the ice lip increases the difficulty of oil cleanup since oil hides under the lip and cannot be burned. Ultimately, this forms an “unrecoverable” fraction of oil which is also hard to reach by mechanical recovery procedure afterwards. The fraction of the unrecoverable oil to original oil amount for each size of ice cavity was calculated by assuming the thickness of crude oil at extinction is 2 mm and shown in Table 8. Two aspects are noted:

1. The unrecoverable fraction of oil after a burn in an ice cavity is a function of the initial *L/H* ratio.
2. For the same thickness (1.5 cm) both intermediate and small-scale tests show similar values of the unrecoverable fraction (~11.5 %).

Tests in the small-scale have showed that by choosing a right ratio of ullage to oil thickness, the “lip” can be avoided (or melted) as the fuel surface lifts up to reach the top of the ice cavity. The onset of cavity formation and the corresponding controlling parameters related to its growth during the burn are new and unexplored questions in fire research. In other words, the answer to questions of when does lateral cavity formation take place and how does it take place will open new doors to our fundamental understanding of liquid fuel fires. From a practical point of view, it was experimentally shown that for both small and large-scale burning, the formation of the lateral cavities alone causes a minimum 11 – 35 % decline in burn efficiency. Such a drop may be unacceptable in an environmentally fragile environment such as the Arctic, where long-term pollution may have adverse effects.

7. Mathematical model

The burning of a pool fire can be modeled if the relevant heat transfer conditions and corresponding vaporization/mass burning rate are known. In the case of a liquid pool in an ice channel/cavity, the melting of channel walls causes additional heat transfer processes to interact with the burning behavior as shown in Fig. 42.

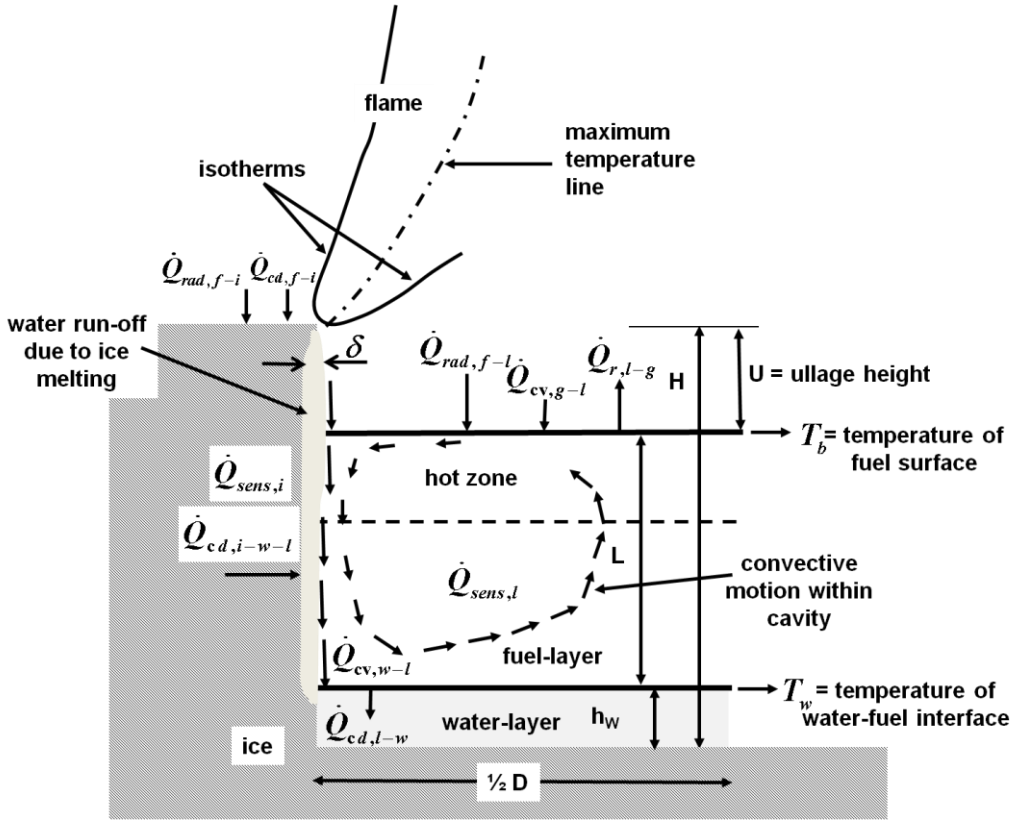

Fig. 42: Schematic of the heat transfer processes during the burning of a combustible liquid in an ice cavity (*Subscripts: cv = convective, cd = conductive, rad = radiative, f = flame, i = ice, l = liquid (fuel), g = gas, w = water*)

These processes coupled with the change in geometry of the vaporizing boundary of the liquid (because of melting ice) will cause changes to the burning behavior normally observed in pool fires. The mass loss rate may never reach a steady state before the extinction because of the geometry change. The small-scale tests in this study systematically characterized the heat transfer mechanisms because of the interaction of an oil layer with a water, cold rigid boundary, and cold nonrigid boundary (ice).

The experimental results from the current study as well as prior theoretical work on the subject of pool fires [14-20] is used to derive and evaluate an overall energy balance to obtain an expression for the burning rate. Mechanisms in which the heat losses function in and out of fuel layer are depicted in Fig. 42. The heat flux received by the fuel layer comprises of convective ($\dot{Q}_{cv,g-l}$), and radiative ($\dot{Q}_{rad,f-l}$) heating supplied by the flame. As shown in Fig. 42, the flame also supplies heat ($\dot{Q}_{cd,f-i}$ and $\dot{Q}_{rad,f-i}$) to the ice causing it to melt and the consequent water enters the cavity and accumulates at the bottom forming a water sub layer of height h_w. $\dot{Q}_{sens,i}$ denotes the sensible and latent heat of ice necessary for the phase change of ice to water. As burning continues, the water layer increases thereby causing the fuel layer to rise up in the cavity and decrease

the ullage height *U*. The ice melting will also cause the shape of the cavity to change with time. The cavity size will increase mainly near the fame anchoring point (flame leading edge). This will cause the fuel layer to stretch laterally thereby reducing its thickness (*L*). The melted water layer falling down the ice wall has a thickness denoted by δ in Fig. 42. The term $\dot{Q}_{r,l-g}$ denotes the heat loss via surface re-radiation and reflection from the fuel surface.

In-depth conduction ($\dot{Q}_{cd,l-w}$) to underlying cold water encompasses a significant portion of the heat loss. Compared with fires in a confined vessel, this heat loss is enhanced because of the changing shape of the cavity (increase in diameter) as discussed previously. $\dot{Q}_{cd,l-w}$ is a function of the fuel layer thickness (*L*), and temperatures of fuel surface and fuel-water interface represented as T_b and T_w in Fig. 42. Both thickness (*L*) and T_w are influenced by the melting ice and corresponding change in the fuel layer geometry. The conductive term, $\dot{Q}_{cd,l-i}$, represents the heat losses to the surrounding icy walls.

Compared with fires in confined metal vessels where heat conduction through vessel-rims contributes to temperature rise of fuel layer, icy walls act in an opposite fashion and significantly cool the fuel layer via lateral conduction of heat. If the heat transfer is high enough, which is possible if the fuel boiling points are high, further melting of ice occurs thereby increasing δ and h_w and decreasing *U*. Convective transport ($\dot{Q}_{cv,l-i}$) can comprise of natural convection (driven by buoyancy forces) and Marangoni convection (driven by surface tension difference). The latter is especially important in this environment because there exist significant temperature differences (ANS crude oil surface temperatures are ~ 120 – 350ºC and ice temperature can be ~-30ºC or lower!).

Finally, $\dot{Q}_{sens,l}$ denotes the sensible and latent heat energy that is used up by the fuel layer to vaporize. This term expressed as $\dot{m}L_v$ is used to obtain an expression of the mass burning rate and discussed next.

7.1 Model formulation

There have been numerous attempts to model heat losses from fuel layer to underlying water in pan fires [2, 7, 14, 21-23]. Similar to these studies, an expression for the energy balance of the fuel layer is used to estimate burning rate of crude oil in an ice cavity. The results from the model are then compared with experimental results for different cavity sizes (5 - 100 cm) to validate the efficiency of the model. The following simplifying assumptions are made:

1. Convective motion within the liquid ($\dot{Q}_{cv,l-i}$) is ignored. This is because this term is most difficult to quantify or measure experimentally. Note that it will weakly affect the fuel layer when burning high viscosity fuels, and perhaps it may be reasonable for the ANS crude oil which is highly viscous.
2. Reflection and re-radiation from the surface is ignored ($\dot{Q}_{r,l-g}$)
3. The ullage effect is ignored. In other words, we do not take into account the increase in the burning rate that may be caused because of the rise of the fuel layer because of melting of water in the cavity.
4. Constant properties are used in the model (ρ, ρ_∞, C_p, L_v). Thermal conductivity of crude is a function of temperature and composition. These effects are ignored and a constant thermal conductivity calculated at 200 ºC is assumed.
5. The geometry of the ice cavity changes with time. It is assumed that this change is linear.

6. The formation of the ice lip or lateral ice cavity is not accounted.
7. The in-depth fuel layer temperature profile is assumed to be linear. In other words, knowing temperature of the fuel surface, fuel-water interface, and the thickness of the fuel layer is sufficient to quantify the in-depth losses via conduction.
8. The influence of the film of water on the wall of the ice on the heat and mass transfer process is ignored.

Given assumptions 1 – 8, the energy balance of the fuel surface can be written as:

$$\dot{Q}_{s,f-l}(t) - \dot{Q}_{cd,l-w}(t) - \dot{Q}_{cd,l-i}(t) - \dot{m}(t)L_v = 0 \quad (5)$$

Where $\dot{Q}_{s,f-l}$ is the net heat flux per unit area reaching the surface, $\dot{Q}_{cd,l-w}$ is the net heat conducted to water sub-layer, $\dot{Q}_{cd,l-i}$ is the net heat loss by conduction to icy walls and $\dot{m}L_v$ denotes the mass burning rate multiplied by the heat of gasification. A sketch of the simplified energy balance at the fuel layer is shown in Fig. 43. Note that the heat feedback from the flame to the fuel surface ($\dot{Q}_{cv,f-l}$ and $\dot{Q}_{rad,f-l}$) is combined and denoted by $\dot{Q}_{s,f-l}$.

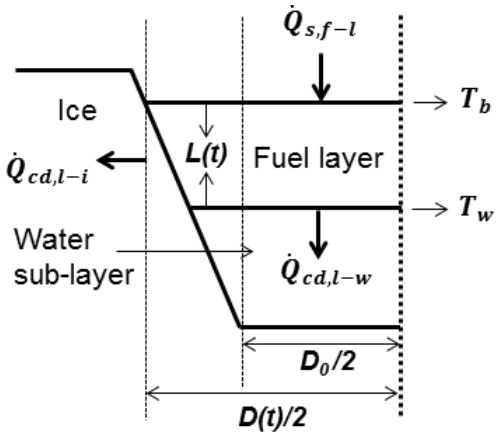

Fig. 43: Simplified view of heat transfer mechanisms involved in the fuel layer

The heat balance is similar to that used in classic pool fire literature [7] except for two main differences:

1. The term, $\dot{Q}_{cd,l-i}$, which denotes the heat loss by conduction from the side of the fuel layer is typically positive as heat is usually conducted from the vessel rims to the fuel.
2. All the heat transfer terms depend on the changes in the cavity and fuel layer geometries. Thus, modeling the distribution of heat transfer from the flame to the liquid surface has to account for the change in cavity geometry.

Given the two differences, each term in Eq. 5 is further explained below:

The flame heat flux ($\dot{Q}_{s,f-l}(t)$):

Torero et al. [24] is used to express the flame heat flux. The expression is similar to that used by others as well [7, 25], and the heat flux reaching the surface can be expressed as:

$$\dot{Q}_{s,f-l}(t) = \chi\, \rho_\infty C_p \left[T_\infty g\left(T_f - T_\infty\right)\right]^{\frac{1}{2}} D(t)^{5/2}, \quad (6)$$

where ρ_∞, C_p, and T_∞ are properties of air at ambient temperature; T_f is the temperature of hot gases above the liquid and is assumed to be constant (1100 K) [24]; χ represents the fraction of the total heat release fed back to the fuel surface. Similar to Torero et al. [24] χ is assumed to be a constant and is equal to 5×10^{-3} irrespective of size of the fire. The changes in the diameter of cavity, $D(t)$, and the thickness of the fuel layer, $L(t)$, are obtained experimentally from the small-scale test data performed using 5 and 10 cm initial diameter cavities.

Experimental data show that the change in diameter *D(t)* and fuel layer thickness *L(t)* (Fig. 15 a and b shown below once again for convenience) follow an approximately linear trend with respect to time (at + b) where "a" equals to $\frac{Final-Initial}{time}$ and "b" is the initial value.

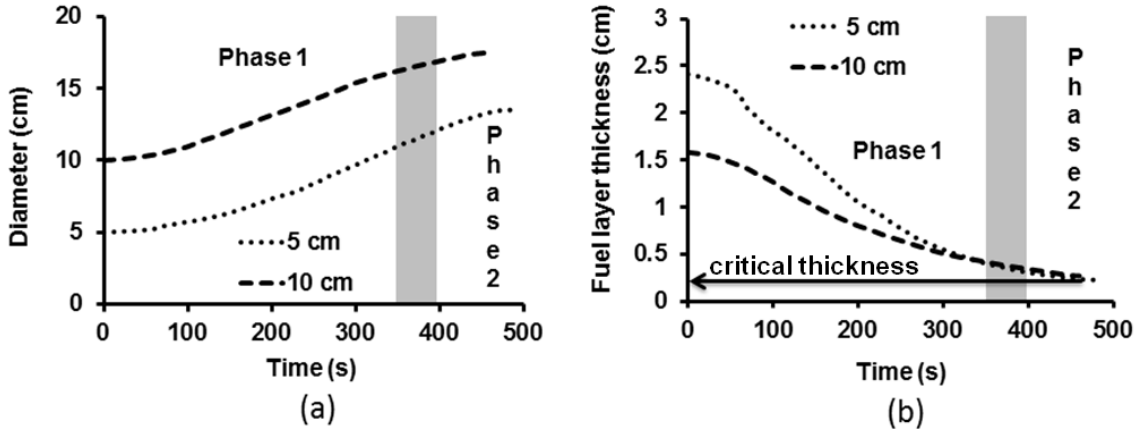

Fig. 15: a) Expansion of ice cavity in course of combustion. b) Fuel layer thickness decline. The arrow is indicating the terminal fuel layer thickness.

If a linear increase in diameter and decrease in thickness is assumed, three input parameters of an initial value, final value and the time duration of the burn are required to formulate an expression for *D(t)* and *L(t).* Since the change in diameter is not significant as size increases, or in other words, the expansion of the ice cavity decreases with increasing scale, it is expected that this assumption should improve from small to large-scale.

In-depth conduction ($\dot{Q}_{cd,l-w}(t)$)

As the fuel layer burns it thins thereby increasing the heat loss to the water sublayer below. This heat loss is mostly because of conduction from the fuel surface which is close to the boiling point (~120 to 400 ºC) and the water-fuel interface which can be anywhere from 0 to 100 ºC depending on the temperature of the water. The loss term represented by $\dot{Q}_{cd,l-w}(t)$ is given by:

$$\dot{Q}_{cd,l-w}(t) = \pi \left(\frac{D(t)^2}{4}\right) \left(\frac{\lambda_l}{L(t)}\right) (T_b(t) - T_w(t)), \qquad (7)$$

where, λ_l is the thermal conductivity of the fuel and is assumed to be constant. For the small-scale tests, $T_b(t)$ and $T_w(t)$ are obtained experimentally as shown in Fig. 20. $T_b(t)$ and $T_w(t)$ for the 10 cm trial were time averaged and used as constant values in modeling the intermediate and large-scale trials (assumption 7). Since boil over occurs at diameters > 25 cm, it is assumed that T_w equals 100ºC at the onset of boil over for these cases. The time to boil over is obtained experimentally.

Conduction to icy walls ($\dot{Q}_{cd,l-i}(t)$)

The conduction to icy walls is also a source of heat loss, especially during the early stage of combustion when the fuel layer is relatively thick and surface in contact with ice is larger. This term is calculated by assuming that the fuel layer comprises of a cylinder of diameter *D*(t) and height *L*(t). The curved surface area of the cylinder is then estimated from simple geometry and the heat loss to icy walls is calculated as:

$$\dot{Q}_{cd,l-i}(t) = \frac{\lambda_l}{\frac{D(t)}{2}} (2\,\pi(\frac{D(t)}{2})\,L(t))\,(\frac{T_b+T_w}{2}(t) - T_{ice}). \quad (8)$$

The temperature at the center of the fuel layer is assumed to be the average between $T_b(t)$ and $T_w(t)$ while the temperature of icy walls, T_{ice}, is assumed to equal to 0 ºC.

Mass loss rate

The mass loss rate can be obtained by combining Eq. (5-8) as:

$$\dot{m}(t) = \frac{\dot{Q}_{s,f-l}(t) - \dot{Q}_{cd,l-w}(t) - \dot{Q}_{cd,l-i}(t)}{L_v}. \quad (9)$$

Eq. 9 is used to obtain the mass loss rate of a liquid fuel in an ice-cavity. Property data used in the estimation are given in Appendix A.

7.2 Model results

Mass loss rate vs. time

Figure 44 shows the experimental and calculated mass burning rate for the 5 cm and 10 cm diameter ice cavities with ANS crude oil. As shown in Fig. 44 the model does a reasonable job at predicting the mass loss rate vs. time.

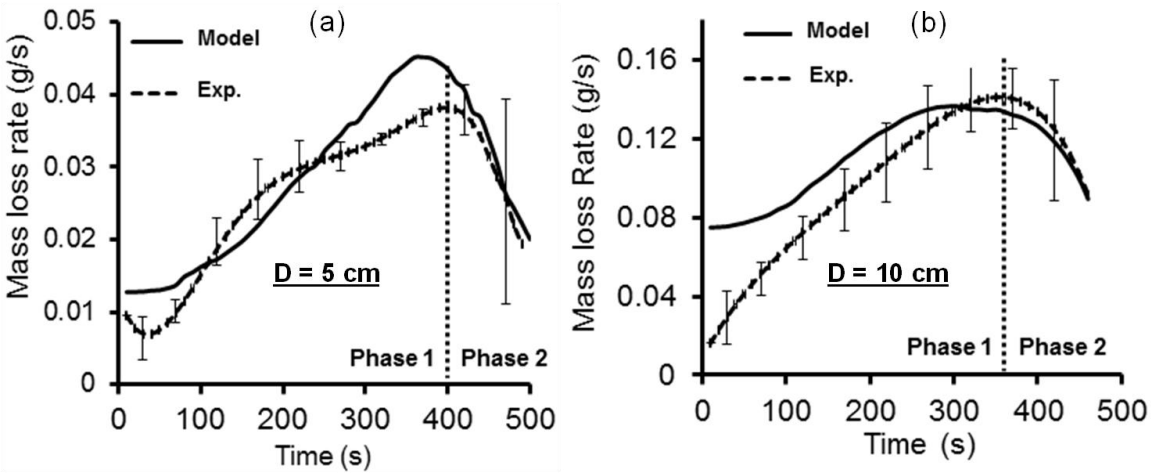

Fig. 44: Mass loss rate vs. time for small scale tests. Comparison of experiments with model (a) D = 5 cm, (b) = 10 cm.

Both phase 1 and phase 2 are captured by the model. The over-prediction during initial stages, as shown in Fig. 44, is mainly because of ignored effect of ullage (assumption 3). After the elevation of the fuel layer by ice melting, the ullage decreases resulting in a more effective burning of the fuel. During phase 2, the fuel layer penetrates into the ice,

creating an ice lip (small lateral cavity). This effect has not been modeled and may be the cause of the lack of agreement by the model and experiments in this stage. The ice lip conceals a certain quantity of the liquid fuel from the heat flux from the flame, causing a reduction in combustion efficiency.

Average mass loss rate for intermediate and large-scale tests

The average regression rate (triangular symbols) is compared with experimental data as shown in Fig. 45 which is repeated from Section 6.

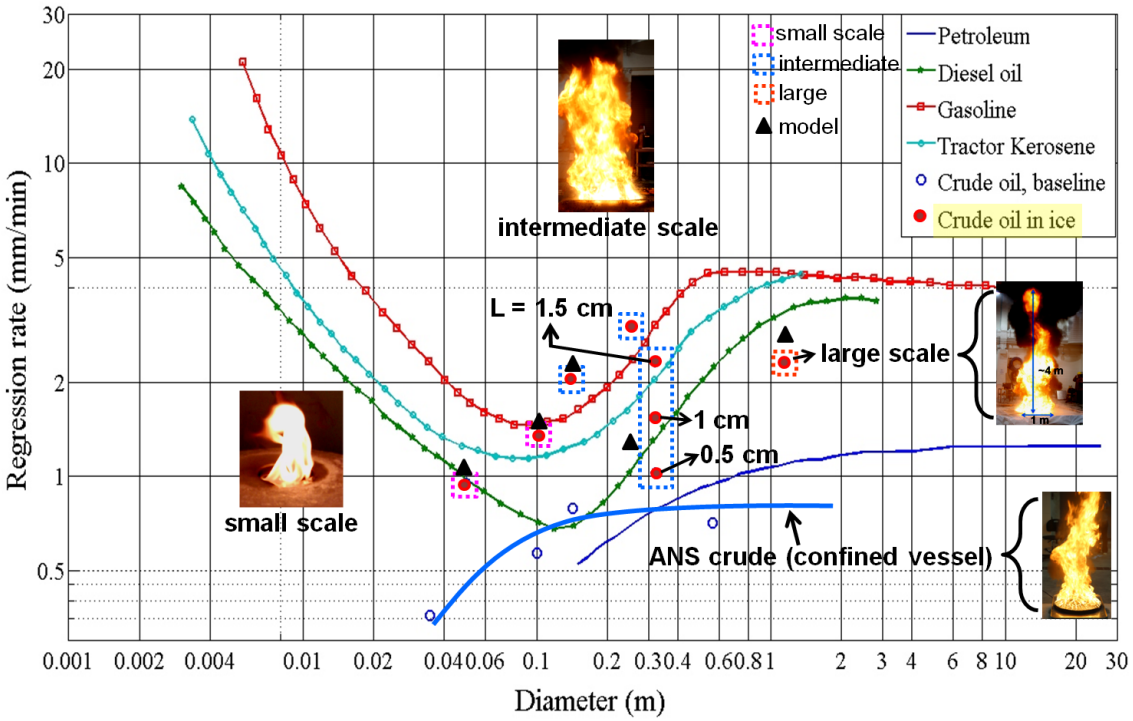

Fig. 45: Regression rates of crude oil in various sizes: Comparison of model (triangular symbol) with experimental data (red circles)

As shown in Fig. 45, the model and experimental results show good agreement. This is promising. However, further work is necessary to improve the model as it over predicts the average regression rate currently. Further, the model heavily relies on experimental input data which may not be possible to obtain in the field. Some assumptions used in deriving the model are also questionable and require further investigation.

Burning efficiency

Fig. 46 compares the experimentally obtained burning efficiencies with the mathematical model. The burning efficiencies calculated by the model are in agreement with the experimental. The reason for the under-prediction of the model for the 25 cm trial is not resolved.

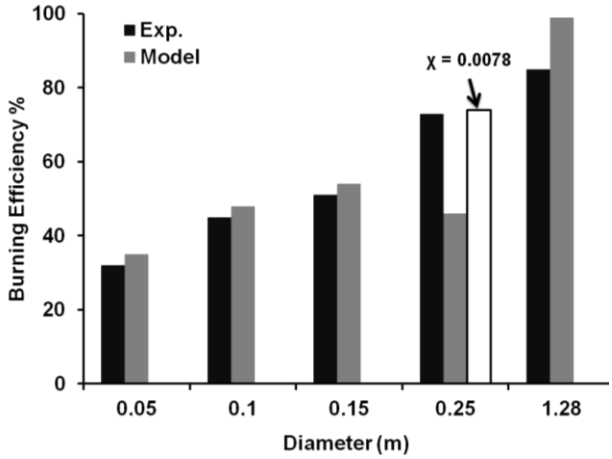

Fig. 46: Burning efficiency-Experimental vs. model comparison

The influence of the fraction of heat fed back to the fuel (χ) is shown in Fig. 46 by making χ equal 7.8×10^{-3} (~ 50% increase). On doing so, the efficiency matches the experimental value. This exercise demonstrates the need to improve our understanding of input parameters and develop a *guide* that can be applied towards estimation of parameters required for mathematically modeling burning behavior under such situations.

7.3 Model limitations and cautionary note

The model formulated in this study is a first step towards predicting the burning rate of an oil spill in an ice cavity. Significant modification to existing pool fire models in the form of geometry changes and lateral conduction losses have been incorporated. However, several assumptions than were used in deriving the energy balance need further study. Chief among them is the value assigned to χ, which was assumed to be a constant. The assumption of constant properties may also result in discrepancies between the model predictions and the experimental values because of the multicomponent nature of the crude oil. It will therefore be necessary to develop bench-scale testing platforms to provide material properties (λ_l, ρ_l) of crude oil as a function of temperature. Towards this end, the use of a newly developed Crude Oil Flammability Apparatus (COFA) was recently demonstrated by Brogaard et al. [26]. The COFA is a bench scale experimental setup designed to represent realistic full-scale conditions such that extracted flammability parameters can be transferred directly to the field.

8. Conclusions and future work

A series of experiments were conducted to develop an understanding of the burning of crude oil in ice cavities. Specifically, Alaska North Slope (ANS) crude oil (~1.5 cm thick) within ice cavities of diameters (5 – 100 cm) and height 6 - 25 cm were studied. A predictive model encompassing the main heat transfer mechanisms, to solve for mass burning rate was also developed. Though simplified, the model is a first step towards analyzing the various heat and mass transfer processes in a systematic way. The following major experimental findings were obtained:

1. Overall, the average burning rate in an ice cavity is greater than that of a similar sized vessel or a pan. This is because the mass burning rate is enhanced by the expansion of the cavity diameter due to the melting of ice. As the diameter of the cavity increases, the fuel also stretches laterally thereby reducing in thickness. The melted ice water causes the oil layer to rise up, which causes the ullage to decrease. The reduction in ullage and increase in diameter counteract the reduction in thickness because of the widening of the fuel layer.

2. The icy walls create a heat sink effect. This effect was found to be more prominent for the smaller diameter cavities (5 and 10 cm). For the larger diameters (15 to 100 cm), the in-depth heat conduction losses to the cold water below the oil layer are more dominant.

3. The critical thickness of the crude oil layer at extinction was equal to 3 mm for 5, 10 and 15 cm diameter cavities. For the 25 cm cavity, the critical thickness equals 1 mm. For the 100 cm cavity, the critical thickness equals 3 mm.

4. Boil over was observed for cavity sizes larger than 25 cm.

5. In all cavity sizes, a lateral cavity similar to that reported in Bellino et al. [13] was observed. The lateral cavity causes 10 - 35% of the crude oil to be trapped inside the ice wall. Understanding and predicting the formation of this lateral cavity is an important consideration in *insitu* burn applications in the field.

A few areas related to the problem of burning a fuel in an ice cavity need to be further explored. The areas are identified based on the urgent need for a predictive model that can estimate the ignitability and burning efficiency based on input parameters that are previously known (or measured). These parameters include oil properties (ρ, C_p, L_v, T_b, λ_l), initial geometry and temperature and a means to estimate the radiative fraction, and particulates. Towards this end, the use of a newly developed Crude Oil Flammability Apparatus (COFA) was recently demonstrated by Brogaard et al. [26]. The COFA is a bench scale experimental setup designed to represent realistic full-scale conditions such that extracted flammability parameters can be transferred directly to the field. The extension of such a flammability apparatus towards an Arctic setting is needed.

The critical ratio identified as the thickness of the spill (*L*) divided by the height of the cavity (*H*), plays a significant role in the average burning rate. Further tests especially at the large-scale (1 x 1m) need to be performed to analyze the sensitivity of this parameter to burning rate and efficiency.

The experimental set up used to investigate the change in geometry of the ice cavity with the addition of external heat flux was specifically designed for this experimental program. The basic idea was to separate or decouple the flame from the problem. In other words, the question of what would happen if a fuel in an ice cavity were exposed to

a constant heat flux without the consequent burning was addressed. It was shown that heat fluxes of 30 - 50 kW/m^2 produce similar geometry changes without the presence of the flame. Further tests with larger diameters and different critical ratios need to be performed to further explore these phenomena. Also note that a minimum size (thickness, diameter) is necessary to provide sufficient radiative heat feedback to the fuel surface for it to burn. Flame spread studies allows this evaluation, since it's only when a flame can successfully spread can sustained burning of fuel occur. The first fundamental step in the analysis of flame spread is analyzing ignition. The radiative heating apparatus allows systematically studying this aspect of the problem as well.

Tests in the small-scale have showed that by choosing a right ratio of ullage to oil thickness, the “lip” can be avoided (or melted) as the fuel surface lifts up to reach the top of the ice cavity. In other words, the lateral cavity formation can be avoided by choosing the optimum initial geometry condition. The onset of cavity formation and the corresponding controlling parameters related to its growth during the burn are new and unexplored questions in the area of fire research. In other words, the answer to questions of when does lateral cavity formation take place and how does it take place will open new doors to our fundamental understanding of liquid fuel fires. From a practical point of view, it was experimentally shown that for both small and large-scale burning, the formation of the lateral cavities alone causes a minimum 11 – 35 % reduction in burn efficiency. Such a reduction may be unacceptable in a fragile ecosystem of the Arctic, where long-term pollution may have adverse effects. The question of quantifying this impact on the fragile arctic ecosystem (both atmospheric and surface) in the form of plume dispersion, consequent particulate buildup in the atmosphere and burned oil residue left over in the water-ice mixture is a future concern and consequent direction that needs work.

Appendix A. Property data

Table A.1: Property of combustible liquids used in this study

	n-Octane	m-Xylene	Dodecane	Crude Oil
Formula	C_8H_{18}	C_8H_{10}	$C_{12}H_{26}$	-
MW	114	106	170	-
Liquid Density (kg/m^3)	708	860	753	866
Viscosity (centi-poise, cP) @ 25°C	0.51	0.62	1.4	11.04 (@ 20°C)
Flashpoint (°C)	13	25	71	25 - 35ºC
Firepoint (°C)	20	44	103	-
Boiling Point (°C)	125.7	139	216	38 – 570 ºC
Thermal Conductivity k (W/m-K)	0.147 (@300K)	0.159/0.132 (@293K/273K)	0.14 (@300K)	0.14
Specific Heat Cp (kJ/kg-K) @ 25°C	2.15	1.72	2.21	2.2
Heat of Combustion ΔHc (kJ/g) @ 25°C	44.44	40.82	44.46	44.77
Latent Heat Lv (kJ/kg)	300	343	256	250
B-number (in air @ 20°C)	5.2	5.8		
Oxygen/Fuel Mass Ratio	3.502	3.165		

Note: All the properties are from the SFPE handbook.

Temperature related Properties

(coefficients used in calculation are also listed)

T (K)	300			
Viscosity (cP)	0.5 [1]	0.58 [1]	1.38 [1]	
Specific Heat Cp (kJ/kg-K)	1.697 [2]			
Thermal Conductivity k (W/m-K)	0.0135 [2]	0.138		

[1]. “The properties of gases and liquids”, Table 9-8.

[2]. “Introduction to Combustion”, Turns.

Viscosity Calc.	**n-Octane**	**m-Xylene**	**Dodecane**	**Crude Oil**
A	-4.333	-	-4.526	
B	1.09E+03	-	1.45E+03	
C	0	-	0	
D	0	-	0	
u @ T_K	-	0.6	-	
T_K	-	298	-	
Thermal Conductivity k Calc.				
A	-	1.64E-01	-	
B	-	-1.47E-05	-	
C	-	-2.39E-07	-	

Appendix B: Baseline test data

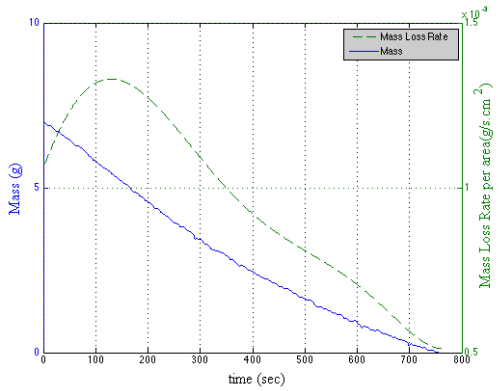

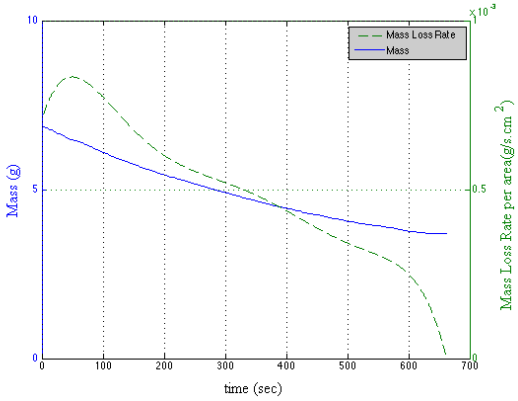

a1) Octane with 3.5 cm ID **a2) Crude oil with 3.5 cm ID**

a1) average mass loss rate = 0.00096 (g/cm^{2}s), peak mass loss rate = 0.0013 (g/cm^{2}s);

a2) average mass loss rate = 0.0005 (g/cm^{2}s), peak mass loss rate = 0.0008 (g/cm^{2}s).

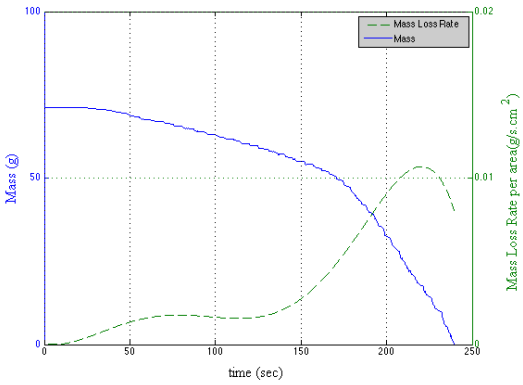

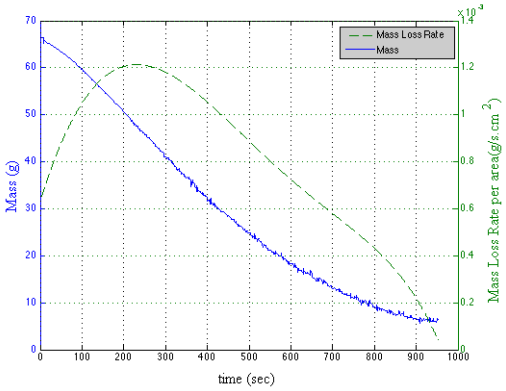

b1) Octane with 10 cm ID **b2) Crude oil with 10 cm ID**

b1) average mass loss rate = 0.0037 (g/cm^{2}s), peak mass loss rate = 0.0107 (g/cm^{2}s);

b2) average mass loss rate = 0.0008 (g/cm^{2}s), peak mass loss rate = 0.0012 (g/cm^{2}s).

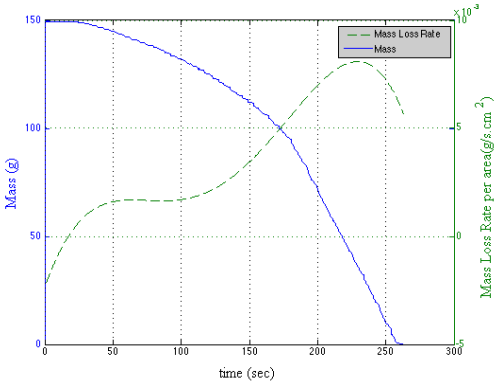

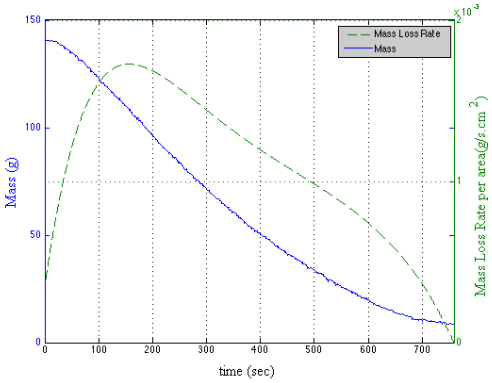

c1) Octane with 14.3 cm ID **c2) Crude oil with 14.3 cm ID**

c1) average mass loss rate = 0.0036 (g/cm^{2}s), peak mass loss rate = 0.0081 (g/cm^{2}s);

c2) average mass loss rate = 0.0011 (g/cm^{2}s), peak mass loss rate = 0.0017 (g/cm^{2}s).

Fig. B1: Octane and crude oil burns in various sized pans in atmosphere.

Baseline data of burning rates under ambient conditions are necessary for comparison with the ones under low temperature conditions. Baseline tests of octane, xylene, and crude oil pool fires in 3.5, 10, 14.2 cm diameter steel pans (1.8 - 2 cm depth) are conducted. The results of octane and crude oil are shown in Fig. B1.

Figure B1 shows that the average mass loss rate of ANS crude oil increases as diameter increases. Ultimately this trend should level out and a constant asymptotic mass burning rate should be reached. For octane this occurs at a diameter of 14 cm itself. The average mass burning rate of crude oil is significantly lower than that of octane (~70% lower). The burning efficiencies of ANS crude oil for the three diameters tested are: 46% (3.5 cm); 91% (10 cm) and 94% (14.2 cm). It will be observed later on that the burning efficiency significantly decreases (~20 – 30%) in icy conditions.

Baseline test of ANS crude oil burn

Fig. B2: Baseline tests (ANS Crude)

Baseline data of burning rate under ambient condition is necessary for comparison with the one under low temperature condition (in ice cavity). For large scale test, baseline test of crude oil pool fire in a 55 cm diameter steel pan (1.5 cm depth) was conducted. 2100 g ANS crude oil (approximately 3 L) was used. Figure B3 shows the mass loss rate curve for 55 cm ANS crude oil pool. The average mass loss rate per area was 0.001 g/cm^2-s.

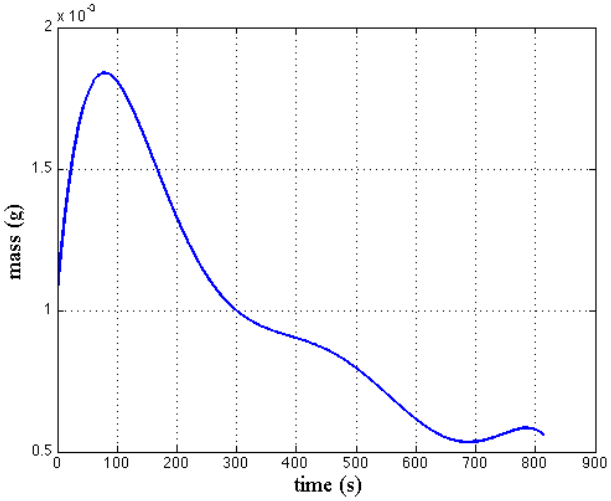

Fig. B3: Crude oil burn in a 55 cm diameter pan in ambient.

Average mass loss rate = 0.001 g/cm^{2}s, peak mass loss rate = 0.0018 g/cm^{2}s.

Appendix C: Spread behavior of oil in an ice channel

An oil spill in ice channel poses unique challenges to that of a spill on water or land. The ice channels are able to transport the oil away from the main mass of the spill making efficient cleanup difficult. To quantify the efficiency of combustion of an oil spill in the arctic environment, the controlling parameters related to the spread of liquid fuels were investigated. Two types of release scenarios have been investigated: instantaneous release (for example the sudden break down of a liquid reservoir), and continuous release (for example a pipe breakage or a hole in a tank whereby liquid flows out of the container at a known flow rate).

C.1.1 Experimental setup

The experimental set up for instantaneous release is shown in Fig. C1. A 24 cm×30 cm×240 cm rectangular acrylic tank has been used as the test platform. For instantaneous release, 24×6×4 cm^3 crude oil (right above the water surface) is originally stored in a 24×61×4 cm^3 container located at the center of the tank. The volume of the crude oil is chosen based on the fact that once released, the final oil-layer thickness will equal 1 mm above the water surface. The container has the same width as the width of the tank so that the release is along the axis of the tank (1-D release). Oil is released instantaneously by lifting the container (Fig. C1).

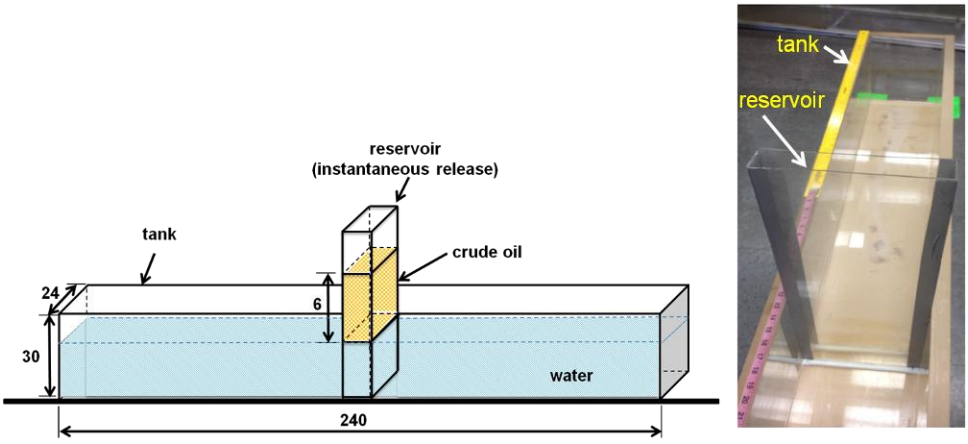

Fig. C1: Experimental setup for instantaneous release

Figure C2 shows the setup of continuous release, oil is released at a controlled constant flow rate from a 0.4 cm inner diameter tube, which is located at the center of the tank and exits at 11.6 cm (h_1) away from the water surface. The same acrylic tank (24 x 30 x 240 cm) is used as the platform for this type of release scenario as well. The flow rate at the exit of the tube is determined by the distance *H* of the fuel surface in the container and the tube exit from where the oil is released. Oil volume in the container is kept constant to maintain a constant flow rate by adjusting the control valve between the reservoir and the container. A reservoir is used as an oil source that is placed on a load cell so that the volumetric flow rate of the oil is recorded.

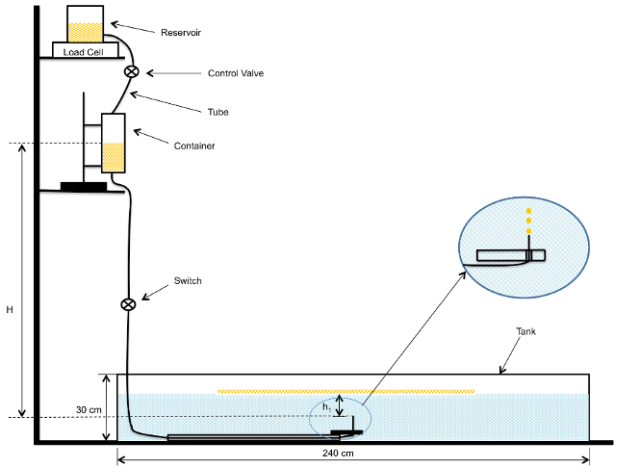

Fig. C 2: Experimental setup of continuous release

For both releases, the displacement of leading edge of the oil is recorded by three video cameras during its spreading. One is placed above the tank for the top view of the release and two are placed beside the long side of the tank and aligned with the water surface horizontally for the side views of two opposite direction releases to capture the oil layer thicknesses. A fourth camera is placed underwater to observe instabilities (if any) between the water and oil layer. For the continuous release setup the flow rate of oil is determined using the mass loss of oil in the reservoir as shown in Fig. C2. The flow rate is controlled by varying the height of the secondary container (Fig. C2).

C.1.2 Experimental results and analysis

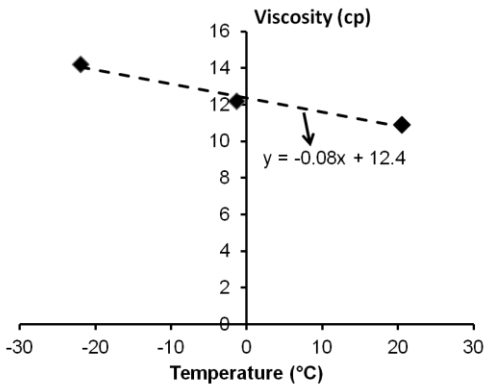

Fig. C3: Viscosity of Alaska North Slope (ANS) crude oil as a function of temperature

Figure C3 shows the viscosities of Alaska North Slope (ANS) crude oil at 20°C, 0°C and -22°C, which are measured by a Brookfield model DV-III+ programmable rheometer with a cone spindle CPE-40. Each measurement requires 0.5 ml of crude oil. The temperature of 0ºC was created by keeping the crude oil in an ice water bath for a few hours. The -22ºC was achieved by using a dry ice (solid CO_2) bath. In both cases, the temperature of the crude oil was taken before and after measurement in the rheometer.

The crude-oil temperature increased after each test, but only slightly (~3ºC). A total of three experiments were performed at each temperature and the standard deviation of the measured viscosity at each temperature is less than 2%. It is observed that, in the temperature range of interest the viscosity of the crude oil increases linearly with a decrease in temperature.

C.1.2 Experimental results for instantaneous release

Two repeated tests of instantaneous release were conducted. The oil (volume = 590ml) was released at the center and spread to both directions along the axis of the tank. Figure C4 shows the change in the shape of the oil leading edge contour as a function of time. Below each image, the labels *t, L* and *h* denote the time (s), distance from the center (cm) and the thickness of the leading edge (mm) respectively. Note that although the initial volume was chosen to be such that a 1 mm thickness spill will cover the entire surface, the maximum thickness that was observed was always more than 1 mm.

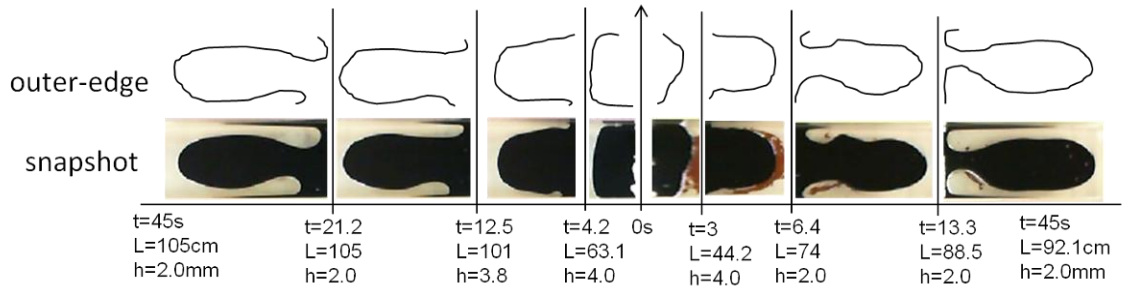

Fig. C4: Leading edge profiles of instantaneous release.

Figure C5 depicts the general behavior of an instantaneous release spill on water. The leading edge races quickly ahead up to about 12 s, after which the spread slows down significantly. As shown in Fig. C5, the quick spread right after the release is denoted as Phase I: 0-10 seconds, which is followed by a slow spread behavior, denoted as Phase II: 10-20 seconds. After this stage, the oil spill tends to recoil such that the distance of the leading edge decreases slightly (Phase III).

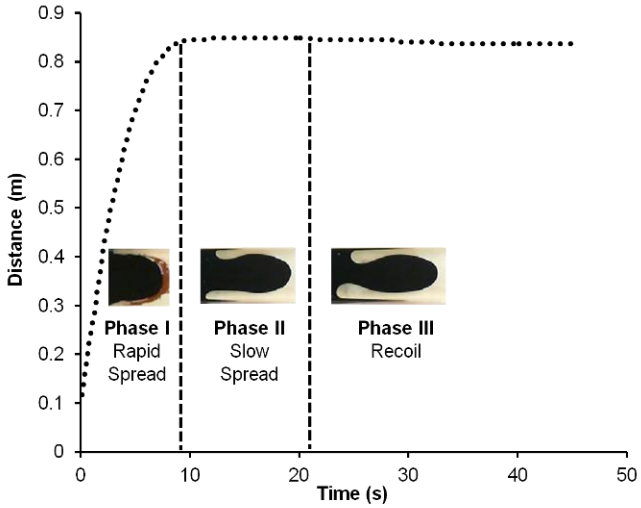

Fig. C5: Phases of instantaneous release

Phase I of the spread can be approximated by a linear trend-line as shown in Fig. C6. A total of four curves are shown along with an average trend line.

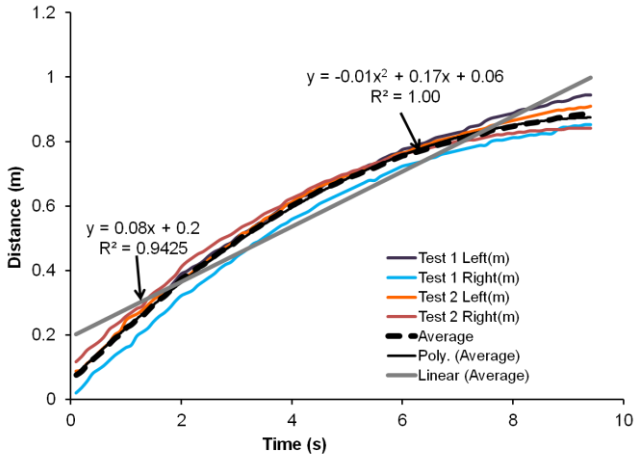

Fig. C 6: Leading edge displacement in Phase I

C.1.3 Experimental results for continuous release

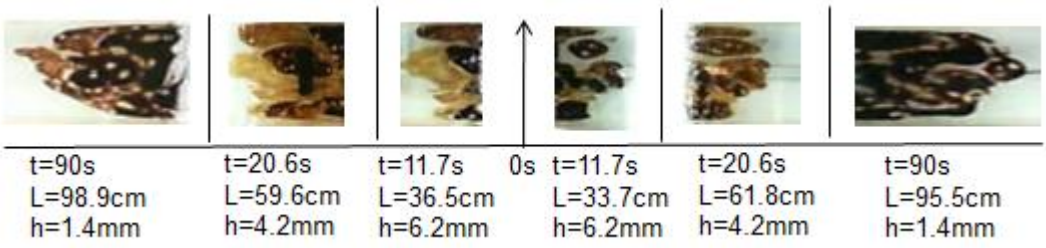

Fig. C 7: Leading edge profiles of continuous release ($\dot{m}''$ = 123 g/m^{2}s)

Three tests of continuous release were conducted at three oil release flow rates as shown in Fig. C7 and Fig. C8. ANS crude oil 550 ml, was used in each trial. Figure C7 shows the profile changing of the oil leading edge as a function of time. Crude oil leading shapes on both sides are symmetrical along the time axis. The profile of the leading is different in comparison to the instantaneous release case. This may be due to the speed of the leading edge as well as the net mass flow rate which is not equal for the two test cases (instantaneous and continuous release). The slope of the instantaneous release tests was 0.08 m/s, and the slope for the continuous release tests varied between 0.02 – 0.04 m/s.

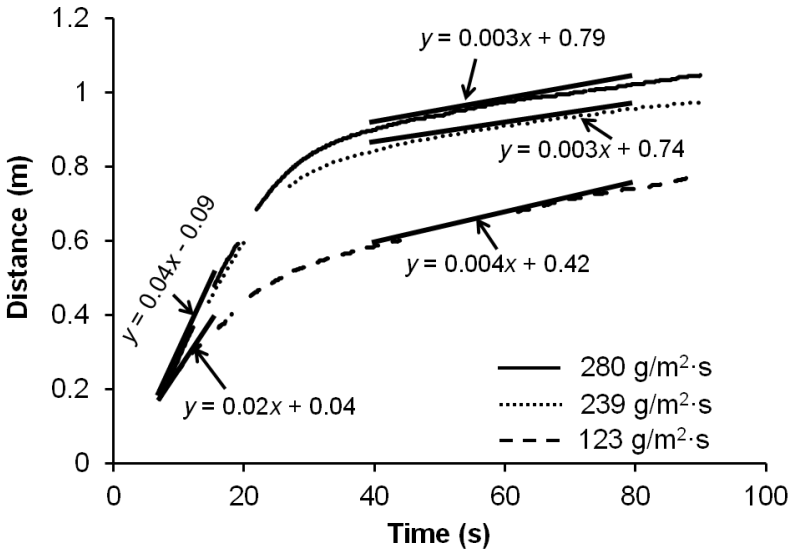

Fig. C 8: Leading edge profiles of continuous release.

Figure C8 shows the leading edge of the spill plotted as a function of time. The spill spreads fairly rapidly initially (for the first 40 s) and then tends to slow down showing a behavior characterized into 2 phases. The “recoil” phase observed in the instantaneous release where the spill tends to retract is not observed in the continuous spill.

C.1.4 Conclusions and future work

An experimental platform for analyzing both instantaneous and continuous releases of crude oil has been constructed. Baseline tests of ANS crude oil spill on water have also been conducted. WPI is currently performing experiments in a channel between two ice walls in setup shown in Figs. C2 and C3. These tests will be compared with the baseline test on water to obtain additional (if any) scaling parameters that will be necessary to model the spread of oil in an ice channel. Ultimately, an engineering model similar to Fay (ref. 3 in the proposal) for oil spills in calm water will be developed.

Appendix D: Fire Science Laboratory Short Form for Short Tests

Test date: 9/25/2013

The purpose of this form is to provide a simple way for students to develop an Experimental Plan for short, uncomplicated tests rather than using the Experimental Plan Template. The numbers listed below match the steps in How to Develop an Experimental Plan. You should read that first to learn how to develop a plan and then use the following format to present it. Short Form in Word Format.

---

1. Background

   Reason for doing experiment:
   To investigate how the low temperature environment (ice condition) will affect the crude oil burning efficiency.

2. Objective

   Data/information you trying to obtain:

   Temperature distribution inside of the fuel/water layer, radiant heat flux of the flame arrived at various locations and the ice cavity geometry change during the oil burning.

3. Process flow and instrumentation diagram (PID)

   Draw your PID:

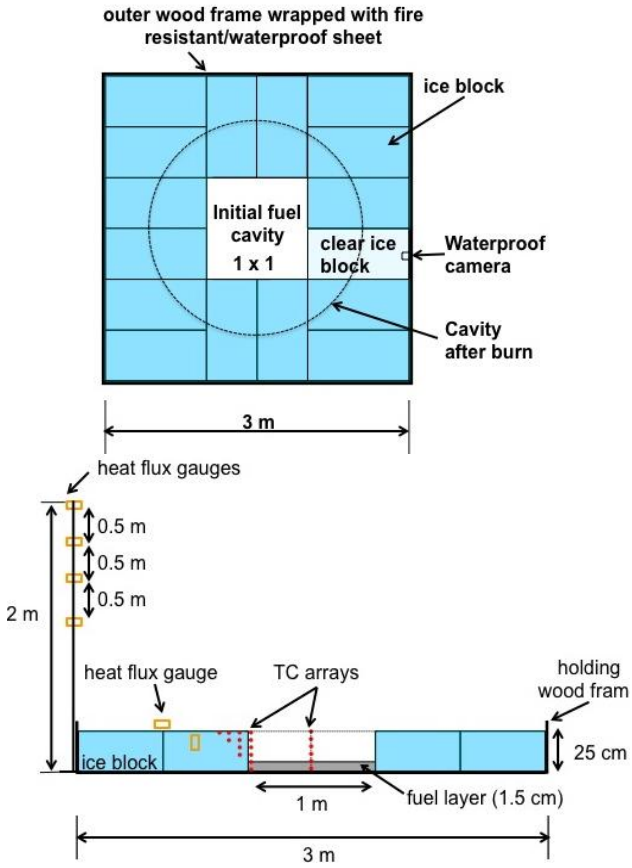

4. PID components

   List components of PID:

   1. 3m (L) x 3m (W) x 0.3m (H) outer container: wood frame wrapped by a 5x6 m^2 fire-resistant sheet and a 6x6 m^2 water proof/flame resistant sheet.
   2. 15 carving ice blocks (1 x 0.5 x 0.25 m^3/each) with 1 clear ice block (same size) Ice blocks will be fused together to prevent the oil from spreading into the gaps. Two methods for fusion will be tried:
      a. **Aluminum sheet method:** Add a heated sheet of Aluminum between the two flat surfaces that need to be fused. Align the ice to desired freezing position then immediately add Ice water around seam to fill in the gaps. Once in place immediately pull out the aluminum. Freezing is almost instantaneous.
      b. **Saw method:** Run the handsaw through the two pieces of ice. The handsaw will bring the two pieces together. Snow will fill in gaps naturally with the sawing action saw. Continue sawing until both pieces meet. If necessary pour ice water onto top piece and watch to see as the water fills the seam. Continue pouring until water completely fills the seam.
   3. A water-proof camera: record fuel layer's rate-of-rise.
   4. The thermocouple trees: measure the temperature distribution and record the movement of the liquid layer.
   5. Heat flux gauges: measure the radiant heat flux from the flame.
   6. A torch with extended arm: ignite the oil.

5. Safety issues

   List materials and chemicals to be used, required use and hazards:

   ANS crude oil: Stored in a standard PGC container meant for Crude oil, and supplied by Aleyska Pipeline, 15 – 17 L of crude oil per test;
   Walking on ice – this will be addressed by placing a rubber mat on the ice during instrumentation phase;
   Saw for cutting.

   List Protective Personal Equipment to be worn to protect against those hazards:

   Safety glasses, fire-resistant gloves, cold protection gloves, masks.
   The ice block will be covered with a rubber mat to avoid slipping during instrumentation stage

6. Failure possibilities

   List failure possibilities of EACH of the PID components and how you will minimize these:

   As a part of the outer container, the wood frame will be completely wrapped by a flame-resistant sheet and also an extra layer of waterproof/flame resistant sheet to prevent any oil or water from leaking. An additional heat resistant blanket if required

7. Checklist

   Write a checklist which encompasses all your procedures: Include pre-test, test and post-test activities Use additional/separate sheet if needed:

   Pre-test:

   1. Check and make sure the hood works properly.
   2. Check and make sure all the heat flux gauges and thermocouples and the data output to computer are working properly.
   3. Check and make sure the water proof camera works properly.

   Test:
   4. The ice will be delivered by Lake Boone ice company. Vendor will carry and assemble ice. Weight of each ice block = 300 lb.
   5. Place the 2 TC arrays at the locations which are pre-marked.
   6. Place the ice blocks into the container to make a 1x1 m^2 cavity.
   7. Fuse the ice blocks together to remove the gaps among them.
   8. Check and make sure the ice cavity has no leaks. The ice blocks have fused. A leak test with water may be performed if there is uncertainty. If this is done remove all water from cavity after leak test using wet vacuums provided by facilities.
   9. Add water into the ice cavity to make a 3-5 cm thick layer on the bottom.
   10. Place the waterproof camera behind the clear ice block.
   11. Add 1.5 cm thick ANS crude oil.

12. Remove rubber floor pads from top of ice
13. Ignite the oil by an igniter with extended arm and let it burn until its self extinguishes.

Post-test:

14. Check the data to make sure everything is saved before disconnecting the instrument/computer connection.
15. Remove the residual oil by 3M oil only absorbent pads. The 3M absorbent pads will remove 99% of the crude oil from the water. Preliminary tests performed in SL 214 (Combustion lab) have shown the pads to achieve this. Data sheet of the pads is also attached. The left over water is therefore considered to be clean.
16. Remove water by wet vacuums.
17. Remove the ice if there's any left and clean the area.
18. The final ice cavity diameter is shown in the sketch. Based on a series of tests conducted earlier, it can be said with confidence that the cavity will not expand to more than 3 m

8. Checklist specifics

Plan to inform others of activities:

BSEE (sponsor)

Number of people needed to run: 8

Lydia Shi (coordinator, WPI, post doc), Peter Bellino (WPI, Phd Student), Brian Elias (WPI, Phd Student), Sreenivasan Ranganathan (WPI, PhD student),Hamed Farahani (WPI, MS Thesis), Ying Zou (WPI MS Thesis), Andre Da Vitoria (WPI Undergraduate), Haoran Li (WPI undergraduate)

9. Emergency shutdown

List events that necessitate an immediate shutdown:

If anything unexpected happens, use CO2 extinguishers to stop fire
Ignition of tarp or wood frame (highly unlikely)
Two trained students with fire extinguishers will be on standby

10. & 11. Apparatus checkout

How will you know if all the components work properly:

Pre check all the components and instruments before running the test

12. Team review

Explain how all team members will know what is going on:

A heads up meeting that will explain the details to the team members.

13. & 14. Pre-test and test

Explain how you will know the information obtained is valid (i.e., reasonable or makes sense):

A baseline test for the large scale burn was conducted on August 30th, several small scale burn tests in ice have been conducted. Results from these tests will be used as reference.

15. Post-test

List what/how you will clean post-test:

1. Remove the residual oil by 3M oil only absorbent pads. A data sheet of the sorbent pads is attached. This is a standard used by industry for oil clean up.
2. Remove water by a pump.
3. Remove the ice if there's any left and clean the area. The ice will be cut into pieces (for easy lifting) and should melt off.

References

1. Garo, J.P., Vantelon, J.P., Gandhi, S., and Torero, J.L. *Some observations on the pre-boilover burning of a slick of oil on water*. 1996. MINISTRY OF SUPPLY AND SERVICES, CANADA.
2. Wu, N., Baker, M., Kolb, G., and Torero, J.L., *Ignition, flame spread and mass burning characteristics of liquid fuels on a water bed.* Spill Science & Technology Bulletin, 1996. **3**(4): p. 209-212.
3. Garo, J., Vantelon, J., and Fernandez-Pello, A. *Boilover burning of oil spilled on water*. in *Symposium (International) on Combustion*. 1994. Elsevier.
4. Buist, I. and Twardus, E. *Burning uncontained oil slicks: Large scale tests and modeling*. in *Proceedings of the Eighth Annual Arctic Marine Oil Spill Program Technical Seminar*. 1985.
5. Garo, J.-P., Koseki, H., Vantelon, J.-P., and Fernandez-Pello, C., *Combustion of liquid fuels floating on water.* Thermal Science, 2007. **11**(2): p. 119-140.
6. Heskestad, G., *Luminous heights of turbulent diffusion flames.* Fire Safety Journal, 1983. **5**(2): p. 103-108.
7. Hamins, A., Kashiwagi, T., and Buch, R.R., *Characteristics of pool fire burning.* ASTM special technical publication, 1996. **1284**: p. 15-41.
8. Gottuk, D.T. and White, D.A., *Liquid fuel fires.* SFPE handbook of fire protection engineering, 2006. **15**(2): p. 297-316.
9. Blinov, V. and Khudyakov, G., *Diffusion burning of liquids*, in *U.S. Army Translation, NTIS No. AD296762*1961, DTIC Document.
10. R., H.A., *Pool burning* Oxidation and Combustion Rev., 1973. **6**: p. 169.
11. Hall, A., *Pool burning: A review*, 1972, Rocket Propulsion Establishment, Westcott (UK).
12. Evans, D.D., Walton, W.D., Notarianni, K.A., Baum, H.R., and Koseki, H. *Large fires: Burning of oil spills*. in *Proceedings of 12th Joint Panel Meeting of the UJNR Panel on Fire Research and Safety*. 2003.
13. Bellino, P., Flynn, M., and Rangwala, A.S., *A study of in-situ burning of crude oil in an ice channe.* Proc. Combust. Inst., 2012. **34**.
14. Nakakuki, A., *Heat transfer in small scale pool fires.* Combustion and flame, 1994. **96**(3): p. 311-324.
15. Hottel, H.C., *Certain laws governing the diffusive burning of liquids.* Fire Res. Abst. Rev., 1959. **1**: p. 41 - 44.
16. Rasbash, D.J., Rogowski, Z.W., and Stark, G.W.V., *Properties of fires of liquids.* Fuel, 1956. **35**(1): p. 94-107.
17. Souil, J.M., Vantelon, J.P., Joulain, P., and Grosshandler, W.L., *Experimental and theoretical study of thermal radiation from freely burning kerosene pool fires.* Dynamics of reactive systems, 1986: p. 388-401.
18. Zhang, X.L., Vantelon, J.P., Joulain, P., and Fernandez-Pello, A.C., *Influence of an external radiant flux on a 15-cm-diameter kerosene pool fire.* Combustion and flame, 1991. **86**(3): p. 237-248.
19. Artemenko, E.S. and Blinov, V.I., *Burning of liquids in vessels with change of level.* Combustion, Explosion, and Shock Waves, 1968. **4**(1): p. 39-42.
20. Orloff, L. and De Ris, J., *Froude modelling of pool fires.* Proc. Combust. Instit., 1982. **19**: p. 885.
21. Emmons, H.W., *Fundamental problems of the free burning fires.* Proc. Combust. Instit., 1965. **10**: p. 951-64.
22. Hottel, H.C. *Certain laws governing diffusive burning of liquids*. 1959.

23. Sher, E., *A theoretical study of the combustion of liquids at a free surface.* Combustion and Flame, 1982. **47**: p. 109-128.
24. Torero, J.L., Olenick, S.M., Garo, J.P., and Vantelon, J.P., *Determination of the burning characteristics of a slick of oil on water.* Spill Science & Technology Bulletin, 2003. **8**(4): p. 379-390.
25. Hristov, J., Planas-Cuchi, E., Arnaldos, J., and Casal, J., *Accidental burning of a fuel layer on a waterbed: A scale analysis of the models predicting the pre-boilover time and tests to published data.* International journal of thermal sciences, 2004. **43**(3): p. 221-239.
26. Brogaard, N.L., Sørensen, M.X., Fritt-Rasmussen, J., Rangwala, A.S., and Jomaas, G. *A new experimental rig for oil burning on water - results for crude and pure oils*. in *Proc. Fire Safety Sci.* 2014. Canterbury, New Zealand, Feb 10-14, 2014. .